CHALMERS

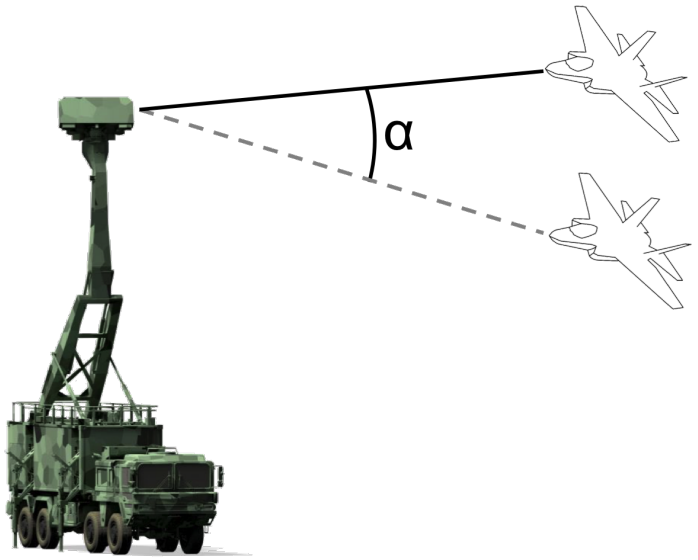

Orientation Estimation of Radar Platforms using MEMS-based Inertial Sensors

Master's Thesis in Systems, Control and Mechatronics

JONATHAN LIDQVIST
BJÖRN SKOGLUND

Department of Signals and systems
Chalmers University of Technology
Gothenburg, Sweden 2015
Master's Thesis EX040/2015

Performance Evaluation of Inertial Navigation Systems in Radar Applications

JONATHAN LIDQVIST
BJÖRN SKOGLUND

Examiner: LENNART SVENSSON
Supervisor: LENNART SVENSSON

Chalmers University of Technology
Department of Signals and Systems
SE-412 96 Gothenburg
Sweden
Telephone: +46 (0)31-772 1000

Department of Signals and Systems
Gothenburg, Sweden. June 2015.

Abstract

A radar observes its surroundings relative to itself in terms of distance and angles. In order to calculate a target's absolute position it is therefore crucial to know the radar's own position and especially its orientation. This is because even a fractional error in the assumed orientation of the radar highly impacts estimated target position. This demand for high accuracy in orientation can be solved by using expensive inertial sensors. But because of their high price and recent developments in sensor hardware technology it has become interesting to investigate the capability of cheaper sensors based on micro electromechanical systems (MEMS) technology.

In this thesis, a MEMS based inertial navigation system (INS) is evaluated and compared in relation to a considerably more expensive INS, which typically can be found in radar systems. The evaluation of the different systems is performed on a non-moving mobile radar system in which the radar antenna is mounted on what can be described as a mast-like construction in order to increase its range. Even if the radar system can be considered as stationary there is still be some minor movement of the radar antenna due to that the mast is mounted on sways back and forth as an effect of the rotating antenna, which is not perfectly balanced. This swaying movement causes the orientation of the radar antenna to vary periodically within a range of angles. In order to not only evaluate the MEMS INS but also investigate how its performance can be enhanced for radar applications, the authors have designed a Kalman filter that tries to make use of the periodic behaviour.

The results show that the designed periodic filter outperforms the existing MEMS INS (under periodic movement). The presented periodic filter design also offers some unique advantages with respect to typical filters used for estimating orientation. Even if the periodic filter described in this thesis does not describe a complete design, including adaptivity to a wider range of periodic behaviours that can change over time, it does suggest that the fundamental design is valid and is suitable for at least a mode of operation if not as a complete filter solution.

Sammanfattning

En radar observerar sin omgivning relativt sin egen position och orientering. För att beräkna ett måls absoluta position är det därför extremt viktigt att veta radarns position och i synnerhet orientering. Detta eftersom även ett mycket litet fel i antagen orientering har stor påverkan på målets skattade position. Dessa höga krav på noggrannhet kan uppfyllas genom att använda dyra tröghetsnavigeringsensorer. På grund av det höga priset och utveckling inom sensor-hårdvara är det intressant att undersöka hur billigare sensorer baserade på MEMS teknologi står sig mot de dyrare systemen.

I den här rapporten utvärderas ett tröghetsnavigeringsystem och jämförs med ett betydligt dyrare system som typiskt används i radarsystem. Utvärderingen utförs på ett stillastående mobilt radarsystem där radarantennen är monterad på en mastlik konstruktion för att öka räckvidden. Även om radarsystemet kan anses stationärt finns det fortfarande en rörelse på antennen eftersom masten svänger fram och tillbaka. Detta på grund av att antennenen inte är perfekt balanserad och snurrar. Svängningen får orienteringen för radarantennen att variera periodiskt inom ett spann på vinklar. Utöver att utvärdera MEMS INS:en har författarna utvecklat ett Kalman filter som använder den periodiska rörelsen för att förbättra mätvärdena.

REsultaten visar att det designade filtret är bättre än den färdiga MEMS INS lösningen(givet en periodisk rörelse). Det periodiska filtret erbjuder även unika fördelar jämfört med typiska filter för orientering. Även om det periodska filtret i den här rapporten inte beskriver en komplett lösning, visar det att det grundläggande konceptet fungerar och är möjlig för åtminstone en del av en komplett lösning.

Acknowledgements

We, the authors, would like to state our most sincere appreciation to Jonas Nordh at Saab for all the assistance provided during the thesis. Without you and your contacts we not have had the possibility to carry out the thesis with anywhere near all the practical elements which made the experience so great.

We would also like to thank others at Saab who assisted us during our practical trials and their facilitation: Fredrik Håkansson, Krister Lyden, Stellan Karlsson, Mats Hansson and Christian Trané.

Finally we would also like to thank Lennart Svensson at Chalmers University of Technology for all his constructive critique and discussions.

Jonathan Lidqvist and Björn Skoglund, Göteborg 17/6/15

Notation

Abbreviations

ARW	Angular random walk
AVAR	Allan variance
BMFLC	Bandlimited multiple fourier linear combiner
DCM	Direct cosine matrix
EKF	extended Kalman filter
FLC	Fourier linear combiner
FOG	fiberoptic gyroscope
IMU	inertial measurement unit
INS	inertial navigation system
LMS	Least mean squares
MEMS	micro-machined electro mechanical sensors
NED	North-east-down
RLG	ring laser gyro
RMSD	Root mean square deviation

Capital Letters

A	amplitude
D	process noise covariance matrix
E	measurement noise covariance matrix
F	transition matrix
H	measurement model
K	Kalman gain
O	observation matrix
P	state covariance matrix
Q	quaternion rotation matrix
R	rotation matrix

Small Letters

a	odd Fourier coefficient
b	even Fourier coefficient
e	error
f	motion function
$\mathbf{g}$	gravity vector
h	measurement function
$\mathbf{q}$	quaternion vector
$\mathbf{w}$	amplitude weight vector
$\mathbf{x}$	state vector
x	x-axis
$\mathbf{y}$	measurement vector
y	y-axis
z	z-axis

Greek Letters

α	misalignment angle
ω	frequency
θ	roll angle
φ	pitch angle
ψ	heading angle
$\boldsymbol{\Theta}$	orientation vector
$\boldsymbol{\delta}$	process noise
$\boldsymbol{\varepsilon}$	measurement noise
μ	bias
ϕ	phase

Subscripts

k	current time
ς	number of roll frequencies
τ	number of pitch frequencies
ν	number of heading frequencies

Superscripts

acc	accelerometer
gyr	gyroscope
p	periodic
s	stationary
t	translational
ref	reference system
sbg	SBG sensor

Diacritical marks

$\hat{}$	approximation or estimate
$\dot{}$	time derivative

Contents

1

INTRODUCTION

The introduction will give some background to why the thesis is needed. The purpose and objective is stated. The scope of the project is explained and to motivate a choice of sensor the introduction also contains a brief market survey. A radar platform and a selected sensor are described to give some background for the evaluations described later in the thesis.

1.1 Background

Saab is Sweden's leading provider of defence and security solutions and is the company that this thesis is performed for. Saab offers a wide variety products and services including radar systems which in in essence is a highly advanced sensor with the purpose to gather intelligence about its surrounding and anything of interest residing therein. Radar applications can be found in the skies as well as at sea and on land. The latter two product segments are included in Saab's battle proven Giraffe line-up, which can be seen exemplified in Figure 1.1.

(a) The Giraffe AMB with the radar antenna located at the top.

(b) The Sea Giraffe AMB with the radar antenna located inside the cone on top of the vessel.

Figure 1.1: Two examples of radar applications from the Girraffe AMB product family by the Swedish defence and security company Saab.

In our ordinary day lives many of us come in contact with radar as a safety function used when reversing our car or when watching the weather forecast on the news. Radar information is in these cases often represented as a top-down view consisting of a two-dimensional image where objects appear to be at a certain distance from the radar sensor. Many of today's radar system such as the high performing Giraffe AMB radar family track targets of interest in three dimensions [1]. Even if the fundamental principals of two- and three-dimensional radar systems are very similar, in that observations are made relative to the radar sensor, a three-dimensional system further increases the need to accurately know the radar antenna's orientation as well as its position in order to calculate the targets position in a global reference frame [2]. The sketches in Figure 1.2 provide a basic impression for the volume, as well as what kind of targets, that can be observed by a radar system.

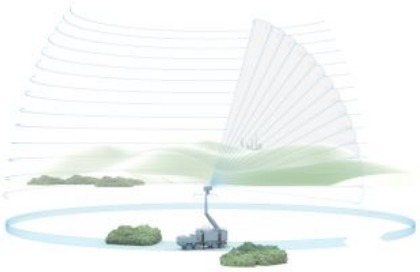

(a) Sketch of the observed volume seen in perspective view.

(b) A section of the observed volume seen in profile along with indicated distances and relevant targets.

Figure 1.2: Sketches depicting the volume observed by a three-dimensional radar.

Even if Figure 1.2 only is an example and the observed volume can differ from radar system to radar system it highlights the vast distances that can exist between the radar and a target. Any errors in the position of the radar system results in a translation of the calculated target position causing an error with same size as that of the radar system's positional error. A small deviation in the orientation of the radar system can however cause a considerably larger error since the long target distances acts as lever arms that can affect the final position of the target severely. As a consequence of this, radar applications requires the orientation and position of the radar system with respect to a global reference frame to be known with great accuracy in order to be able to compensate for any differences.

Inertial navigation systems (INSs) are currently the most common solutions used in order to deal with the issue of estimating the desired orientation and position [2]. A complete INS can estimate both orientation and position based on inertial measurements of rotational rates and accelerations. These measurements are usually provided by gyroscopes and accelerometers but the navigation system can be aided by a wide variety of sensors and systems to observe the surroundings, such as GPS, magnetometers (which acts like a magnetic compass) or even radar to mention a few [3]. By knowing the position of where the radar system is deployed the functional need of the inertial navigation system can be reduced to estimating only the orientation. The thesis is based on this assumption and will therefore focus on the challenge of estimating orientation.

Because of the operational conditions and the required level of accuracy from today's radar systems regarding orientation the used INS consequently comes associated with a high price. Despite it only being a subsystem of the larger radar system the typically used INS has a form factor and power consumption that has to be taken into consideration for the radar system, and thereby also imposes restrictions in terms of overall design.

MEMS-based sensors is a sensor technology that has seen an increase in terms of performance over the last years, and also offers it at a fraction of the cost compared to today's high end inertial navigation systems [4]. Additional benefits of MEMS are also their small size and low power consumption, but price is as in many cases one of the major incentives for considering new technologies. A reduction for the INS cost would not only benefit the overall cost of the radar system but would also allow for new possibilities in reducing downtime due to INS malfunction, which is of utmost importance since lives can depend on a radar system being operational or not. The reduction in downtime might not be obvious but is possible because an inexpensive part or system allows for replacements to be kept in storage, which might not even be an alternative for an expensive system as it would mean tying up to much valuable equity.

1.2 Purpose

The previously explained circumstances bring to mind a very relevant question:

How do available MEMS-based inertial systems perform compared to the high-end systems used in today's radar applications?

Since this currently is unknown the main purpose of this thesis will be to gain insight

regarding existing trade-offs and issues associated with MEMS-based inertial systems for use in radar systems.

1.3 Thesis objective

In order to attain the desired insight the thesis first objective is to evaluate a MEMS-based inertial navigation system by practical trials. These trials should naturally be carried out in an environment resembling that for existing or possible future radar systems so ensure the results are useful in practice. Apart from evaluation of the sensor the thesis will also include exploration of the possibility to develop an inertial system which takes advantage of behaviours typical for radar systems for increasing performance accuracy of estimated orientation.

Both the objectives are to be evaluated by comparing the estimates of orientation from the different systems with those of an inertial navigation system with accuracy similar to that which is found in existing radar applications. The results are also to be compared with parts of the MEMS-based inertial navigation system's specification to verify whether they are met or not.

1.4 Scope

The thesis has some fundamental limitations in terms of available resources. The duration of the thesis is 20 weeks and the authors are the mainly available personnel. A radar system has been made available to the authors by Saab for practical trails but require experienced operators in order to carry out the trials. The radar system is stationary under its typical deployment and the trials are in order to limit evaluated scenarios also be conducted under this presumption. There is no existing MEMS-based INS, which means that a suitable one has to be selected to facilitate all aspects of its installation and usage during trials. The MEMS-based INS can cost no more than 50 KSEK to be within the budget made available by Saab. Further details of the available and selected MEMS-based INS is found in Section 1.5.

To aid in the operation and other practical aspects there is a time budget of 60 working hours to allow employees at Saab to assist the authors. The availability of any employee with relevant knowledge is however not guaranteed since any work pertaining to assistance with the thesis comes secondary to the employees' daily responsibilities.

There exist no requirements to develop a complete implementation in hardware when exploring the possibility to increase the MEMS-based inertial navigation system's performance. The exploration will therefore be carried out by post-processing logged data from the practical trails using MATLAB which provides insight whether the developed concept for the inertial system is valid or not.

1.5 Available radar and selected INS

The radar platform evaluated is one similar to the one in Figure 1.3 and has a high-end inertial navigation system mounted below the rotating radar antenna. This inertial navigation system is considered to be so accurate that it can be considered as measuring the ”true” orientation and is therefore called the reference inertial navigation system. Orientation can be described in relation to an arbitrary frame but the thesis will use the north-east-down (NED) frame as depicted in 1.3. Since the radar platform is stationary and the reference does not rotate with the antenna this means that the reference measures the orientation as the mast of the platform sways due to the rotating antenna and external forces such as wind.

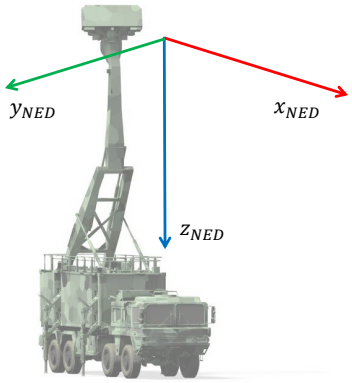

Figure 1.3: The available radar platform and the NED reference orientation frame. Relative to the vehicle the x-axis is defined in the forward direction, the y-axis in the lateral and the z-axis in the downward direction. The orientation consisting of roll, pitch and heading are defined around those axes in the same order.

1.5.1 Choice of sensor

In this thesis a MEMS-based inertial navigation sensor is evaluated and there are several parameters to consider when choosing a sensor. It should of course fit the project budget but it also has to be accurate enough to be used in the considered environment. The INS market is fast growing and accuracy and price of the sensors are ever changing. In this section a brief market overview will be presented to give insight in how the INS market looks and how accuracy affects price, but also other parameters such as user friendliness and size.

1.5.2 Market overview

Inertial navigation systems are usually divided into four main classes depending on price, accuracy and gyroscope technology. These are commonly named Automotive, Industrial, Tactical and Navigation grade [4]. Automotive sensors are as the name implies often used in car applications, but the low end sensors of this class are cheap enough to use in toys and smartphones. Automotive sensors are often individual rate and acceleration sensors and an Industrial INS can be achieved by combining several of these to achieve angular measurements. When high accuracy in orientation is needed the more expensive solutions in the Tactical graded sensors are used. Navigation graded sensors are as the name implies used for navigation, especially in submarines where GPS is not possible. This requires extreme precision in the INS, however these sensors are in practice not used for orientation estimation. Figure 1.4 shows a figure over how the gradings are located in a price/performance graph. This graph is based on [4] and [5] together with data provided from sensor manufacturers. The sensor chosen for this project is one in the price range of Industrial grade.

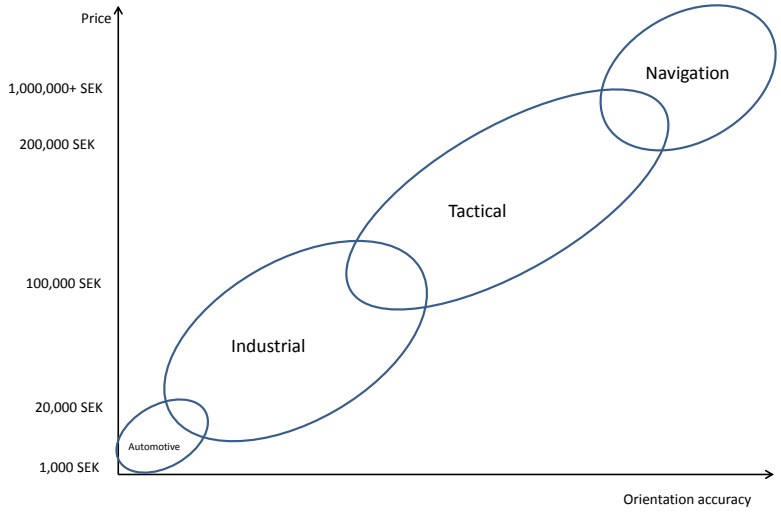

Figure 1.4: Illustration of the different classes of INS.

To give some insight in how INS from different grades perform a simplified table of typical specifications are shown in Table 1.1.

Table 1.1: Approximate accuracies for INS

	Roll/pitch	**Heading**
Industrial	0.1-0.5 °	0.5-1.0 °
Tactical	0.01-0.05 °	0.05 °
Navigation	<0.01 °	<0.05 °

Apart from price and accuracy size is also a parameter that needs to be considered since the size difference between grades is significantly different. Automotive and industrial sensor are exclusively based on MEMS technology explained in Chapter 2, while tactical and navigation graded sensors uses FOG and RLG (two types of gyroscopes that will be discussed later in Chapter 2). This means that an industrial sensor can weigh just a couple of grams (often around 50 g [6]), while a tactical sensor can weigh up to 10 kg [7].

In Table 1.1 it can be noted that the heading angle accuracy is lower than for roll and pitch for all classes of sensors. This is natural because the heading is the hardest angle to measure, for this accelerometers can not be used since they have no information in how the sensor is pointed. In cheaper sensors such as the automotive graded ones, magnetometers measuring the earth's magnetic fields and in that way determining where north is. However this is rarely good enough due to disturbances in the magnetic field caused by wires, metals or electric motors. To overcome this GPS aiding is often added. This means that if the sensor is kept in constant translational motion GPS can be used to determine where the sensor is heading and in extension how it is pointing. This however causes problem if the sensor is not moving, to solve this one has to look in the high end of the price range of industrial graded sensors, where often dual GPS antennas are used. Dual GPS aiding is based on two antennas placed in known position relative the sensor and by using position data from both antennas the heading angle can be determined. For even higher precision in heading a technique used in tactical and navigation graded sensors must be considered. This technique is simply called north seeking and requires extremely accurate gyroscopes (typically RLG) [5]. What north seeking is all about is to basically measure the earth's rotation with the gyroscopes and calculate how the sensor is oriented. Doing so is time consuming but yields very accurate precision in heading.

It is not just heading angle that can be obtained from other sensors. It is common for more expensive INSs to have support from other sensors to aid for example position estimates. This could for example in a moving vehicle be odometers measuring the wheel rotation. Aiding from other sensors is more common in the cheaper sensors up to industrial graded, but of course this cost more.

It is apart from accuracy desirable if the sensor is easy to work with. Good documentation can be very important to make sure that the full capacity of the sensor is retrieved. Smaller, cheaper sensors are often designed to be plug and play and many

companies provide analyzing programs that the user can play around with to get a grasp on how the different sensors inside the INS behaves. For more expensive solutions whole systems can be considered and the manufacturer can adapt the sensor depending on the usage.

1.5.3 Characteristics

Based on the market study performed a suitable sensor was selected and used in the project. The sensor is called Ellipse-N and is developed and manufactured by the french company SBG. This is an industrial grade sensor consisting of MEMS gyroscopes and accelerometers in three axis, magnetometers in three axis and also support for GPS aiding. Ellipse-N contains a predefined EKF that outputs the orientation in Euler angles or quaternions; it is also possible to get the raw measurements from all sensors in different output rates up to 200 Hz. In Table 1.2 the specified RMS accuracy of the sensor is listed [6].

Figure 1.5: The SBG Ellipse-N sensor used in this project.

Table 1.2: Specified RMS accuracy for Ellipse-N. Here 0.8 ° denotes accuracy with magnetometers and 0.5 ° with GPS aiding

	Roll/pitch (RMS)	**Heading (RMS)**
accuracy	0.2 °	0.8/0.5 °

In the filters that are implemented in this project, raw values from gyroscopes and accelerometers are used. In Table 1.3 the specified accuracies for the gyroscopes and the accelerometers are listed in terms of the error parameters described later in Chapter 2.

The constant bias is not listed here since it is different for individual sensors but it can easily be measured or estimated later on.

Table 1.3: Raw sensor specifications for Ellipse-N [6].

	Random walk	Bias instability	Scale factor	Range
accelerometer	100 $\mu g/\sqrt{Hz}$	20 μg	0.1 %	8 g
gyroscope	100 $^\circ/s/\sqrt{Hz}$	8 $^\circ/h$	0.05 %	450 $^\circ/s$

During trials the Ellipse-N with its GPS antenna is attached to a plate which is mounted in close proximity to the reference inertial navigation system. The sensors cannot physically occupy the space and because there are limited options in where to place the Ellipse-N the systems will be misaligned due to limitations of where the sensor can be placed. This misalignment can however be compensated for so that sensors measure the same movement in orientation and can be compared. To read the sensor output a cable is connected from the sensor to a PC that runs a logging program (sbgCenter [8]) provided a development kit purchased with the Ellipse-N.

1.6 Related work

Orientation estimation using inertial sensors is a problem with a wide range with many approaches and solutions. Due to low prices of the MEMS sensors IMUs can be found in all kinds of applications such as toys, cars, and especially mobile phones. In mobile phone technology IMUs are used daily, for example in games and whenever tilting the phone to get a landscape format of the screen instead of portrait the phone sensors estimates the orientation and adapts to suitable format. In areas such as segways and quadrocopters that has grown popular in recent years, IMUs are used to control the orientation.

To solve the problems of orientation estimation there are various methods and filters developed, some are more complex focusing on specific properties while some are more general and easier to interpret.
Madgwick [9] has proposed a filter solution using gyroscopes, accelerometers, and magnetometers that performs well and is widely used. Zhang et al. [10] has for example used it to estimate the attitudes of buoys. For monitoring the oceans a network of antennas placed buoys can be used. For increased communication distance a concept called beam forming can be used, this means that the signal beam energy is concentrated and can thus be directed directly at the target node. The problem of applying this concept on the buoys is that they are constantly moving due to waves and wind. Zhang presents an algorithm that uses the work of Madgwick to estimate the attitude and use it to compensate for the tilt in the beamforming. The algorithm is tested in simulations under the assumption of regular waves and the results showed improvement in antenna gain and distance between nodes.

Tully et al. [11] has developed a method for tracking a heart's moving surface using a camera and Kalman filtering to estimate fast Fourier transform parameters. The implementation was tested on a phantom of a heart and the results showed that the surface was indeed tracked. Further use of periodic filtering is done in the medical area where periodic motion is a common phenomenon. Veluvolu et al [12]. introduces a method of estimating involuntary rhythmic motions(tremor) of body parts using accelerometers and Bandlimited multiple Fourier linear combiner, in this work the designed filter is able to distinguish voluntary motions due to the fact that the frequencies of the tremor is known. A comparison is made between combinations of filters using the BMFLC method and the Kalman filter shows the best results.

1.7 Thesis outline

This thesis begins with an introduction describing the problem formulation and background. In Chapter 2 some general background theory describing concepts that is used. The theory is applied in the modelling and development of filters in Chapter 3. The filters are applied on data collected from the radar platform in Chapter 4 where the performance is presented and discussed. The last Chapter 5 consists conclusions connected to the objectives of the evaluation.

2

BACKGROUND THEORY

This chapter introduces the reader to basic concepts and theory needed to later understand the proposed method and the results. Concepts of Inertial Measurement Units will be discussed and what typical errors this causes. The chapter also gives insight in how filtering works and how periodical motion can be modelled in the filters.

2.1 Sensors

To measure how an object is oriented inertial measurement units (IMUs) are often used. IMU is a collection name for inertial sensors such as gyroscopes and accelerometers. To fully understand inertial sensors the concepts of them need to be explained. In this section the construction and operation of gyroscopes and accelerometers will be explained. Typical errors and specification parameters will also be explained to give insight in how to evaluate the use of a sensor for a certain application.

2.1.1 Gyroscopes

Gyroscopes measures the rate of rotation around an axis, typically three gyroscopes are used to cover rotations around the xyz-axis. There are mainly three types of gyroscope technologies, in this section these technologies will be briefly explained and what the advantages and disadvantages are of each type of sensor. The three technologies are called Micro-machined electro mechanical sensors (MEMS), Fiberoptic gyroscope (FOG) and Ring Laser gyroscope (RLG). The main differences between these types of sensors are: price, size and accuracy of the measurements. These parameters affect the applications where the sensor is meant to operate in; the cheaper sensors are typically used in smartphones and car application while the more expensive sensors can be used in aircraft and military equipment. The three types of gyroscopic sensors are illustrated in Figure 2.1 to give a comparative picture.
The MEMS sensors are manufactured on silicon chips, which mean that they are easy

to manufacture in large quantities and therefore the cheapest of the three types of sensors. The basic concept of MEMS gyroscopes is that they consist of small tuning forks manufactured in silicon vibrating due to the Coriolis effect [13]. The vibration gives rise to a change in capacitance measured and translated to a rotation rate. MEMS sensors are sensitive to changes in temperature since the conductivity of the semiconductor is temperature dependent [14], this is a problem avoided in the more expensive solutions presented next.
FOGs are more accurate but can not be as small as the MEMS. This because the FOG technology is based on a fiberoptic cable arranged as a coil. Light is sent in both directions through the cable and when the sensor is rotated the light moving in the rotation direction will travel faster than the light in opposite direction due to the Sagnac effect [15]. This causes a phase shift that can be observed to determine the angular velocity. The coil needs to consist of a very long optic cable (up to several km [16]) for the phase shift to be big enough to be measured accurately.
RLGs are the most accurate but also the most expensive gyroscopic sensors. It uses the Sagnac effect just like the FOG-sensors but instead of light travelling in an optic cable it has laser beams in two directions and mirrors to guide them. Just as with the FOG the phase shift due to rotation is measured. One disadvantage with RLG is that laser lock-in can occur when the rotation rate is low [17]. To remove this, a motor applying a vibrating dither is used to make sure that the sensor is never completely still. The construction of an RLG therefore needs more mechanical parts and this causes the sensor to increase in size which has to be accounted for in implementation.

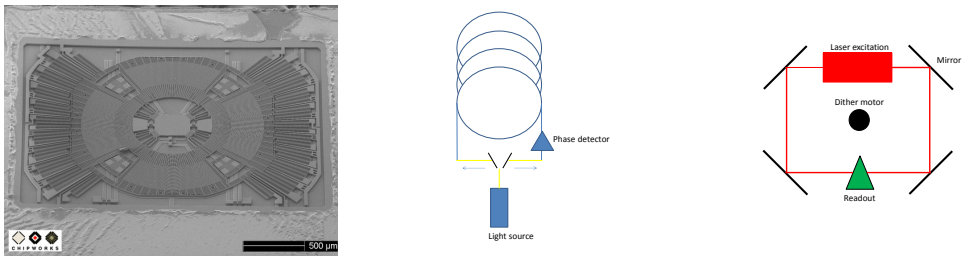

(a) MEMS gyroscope. **(b)** Fiberoptic gyroscope. **(c)** Ringlaser gyroscope.

Figure 2.1: Three different types of gyroscope technology.

2.1.2 Accelerometer

Accelerometers measure the acceleration of an object in typically three axis. An accelerometer behaves as damped mass on a spring, when the object accelerates the mass is displaced. The higher the acceleration is the more the mass is displaced. This behaviour causes an accelerometer to be affected by the gravity acceleration. But the gravity is always pointing toward the center of the earth, so it can be accounted for. The gravity vector can also be used to determine how the object is oriented by calculating the angle of the gravity vector. An accelerometer can also be used to estimate position by integrating the measurements twice; however this causes a second order drift

error. Accelerometers used in electronic devices are of MEMS type. The MEMS accelerometers are basically a small version of damped mass on a spring. The mass is here a moving plate with smaller plates located between fixed plates as seen in Figure 2.2b. When the sensor is accelerated the moving plate will be pressed in the opposite direction like a passenger is pushed to the seat in an accelerating car. This causes a difference in capacitance between C_1 and C_2 that gives rise to a change in voltage v_1 as shown in the figure. v_1 can then be translated to a corresponding acceleration [18]. In Figure 2.2 a MEMS accelerometer and the concept of operation is shown.

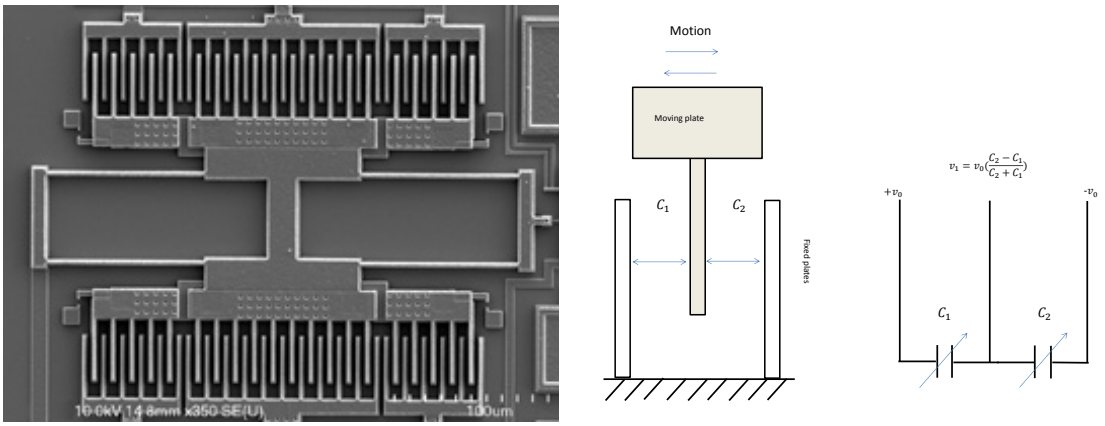

(a) MEMS accelerometer [19].

(b) Concept of a MEMS accelerometer.

Figure 2.2: A MEMS accelerometer and the concept.

2.2 MEMS sensor errors

In this project MEMS sensors are used due to the low cost. To understand how these sensors are specified it can be useful to explain typical errors. To do this simplified models of the sensors are used. A MEMS gyroscope can be modelled in one axis with some simplifications as

$$y^{gyr} = (1 + s^{gyr})\omega^{true} + \mu^{gyr} + n^{hf} + n^{lf}, \tag{2.1}$$

where y^{gyr} is the raw measurement from the sensor and ω^{true} is the true angular rate. The bias is denoted μ^{gyr} and the highfrequent and lowfrequent noise is denoted n^{hf} and n^{lf} respectively. A MEMS accelerometer can be modelled very similarly to a gyroscope with some minor differences as

$$y^{acc} = (1 + s^{acc})a^{true} + \mu^{acc} + n^{hf}. \tag{2.2}$$

Just as in the gyroscope case, a^m is the measured acceleration and a^{true} the true acceleration. The accelerometer is modelled with bias μ^{acc} and assumed to only contain highfrequent noise n^{hf} It can be noted that many of the error parameters are common for both the gyroscope and the accelerometer due to the same type of construction. In

the following sections the error parameters will be explained to give an insight in why measurements from the sensors contain errors and what can be done to separate them.

2.2.1 Scale factor

The scale factor s^{gyr} and s^{acc} is an effect of mis-calibration that causes each measurement to be scaled. Ideally the scale factor should be 0 but this is never the case since the real world is not perfect. For high performance MEMS the scale factor is typically less than 0.05 %.

2.2.2 Constant bias

The constant bias of a gyroscope μ^{gyr} is the mean offset from the true rotation rate. This is easily seen by observing the output values when the gyroscope is still. Since the bias is constant it is easily removed by just subtracting it after it is measured or estimated. The bias of an accelerometer μ^{acc} is a bit harder to distinguish since when the sensor is still it accelerates due to gravity, the constant bias would then be the acceleration in addition to the gravity.

2.2.3 High frequent noise

Angular random walk (ARW) is a way of representing the high frequency noise n^{hf} for a gyroscope. Basically it describes how far the angle measurements would drift away if the angular rate is integrated. When a signal with noise is integrated the integration will drift, how fast it is drifting depends on how much noise the signal contains and it can be shown that the standard deviation of the ARW grows proportionally to the square root of time[20] as

$$\sigma^{ARW} = \sigma_{n^{hf}} \sqrt{T_s t} \tag{2.3}$$

The ARW is expressed in $^\circ/\sqrt{h}$ meaning that a sensor with $ARW = 1$ has an angular drift of 1 $^\circ$ in one hour and $\frac{1}{\sqrt{2}}$ $^\circ$ in two hours and so on. Some manufacturers use different notations of the high frequency noise the most popular notation is the same that is used for high frequent noise in accelerometers the noise spectral density (usually denoted PSD for power spectral density). To convert a PSD to ARW the following formula can be used [21]

$$ARW = \frac{1}{60}\sqrt{PSD} \tag{2.4}$$

For accelerometer the noise is described in the same way as for gyroscopes with the main difference that it is called velocity random walk.

2.2.4 Bias stability

Bias stability is a way of describing the low frequent noise n_{lf} in gyroscopes, basically this describes how the bias in the gyroscope changes over time. The bias stability is small for all gyroscopes and usually expressed in terms of $^\circ/h$. To calculate the bias stability

a method mainly used for expressing stability of clocks but well suited for gyroscopic sensors are used. This method is called Allan variance (AVAR) [22] and is defined as

$$AVAR = \frac{1}{2(n-1)} \sum_i (y(\tau)_{i+1} - y(\tau)_i)^2 \tag{2.5}$$

where the gyroscope signal is divided into bins of length τ seconds. When τ is small $AVAR$ will be mostly dominated by the high frequency noise, but for longer averaging times $AVAR$ reaches a minimum value corresponding to the bias stability [22].

2.3 Rotations of coordinate systems

IMUs are measuring angular rate and acceleration around/in three axis corresponding to a coordinate system of the sensor, which means that the measurements are the values corresponding to the internal axis of the IMU, that is, in the so called sensor frame, S. In this thesis it is not the orientation of the the internal axis that is of interest but rather a fixed global axis such as a coordinate system called North, East, Down frame (NED) defined as in Figure 2.3. To be able to use the measurements from the sensor as orientation relative to the ground they can be represented in the NED frame. The mismatch between NED and S can be seen as a pure rotation. The measurements thus only need to be rotated to express orientation in NED. This section will explain how such rotations can be handled.

2.3.1 Euler and Tait-Bryan angles

To express orientation in three dimensions the most intuitive way is to describe it by three rotations (roll, pitch and heading). This way of representing is called Euler angles. To describe a rotation of a coordinate system relative another fixed system, Euler angles describes it as a rotation sequence around first one axis, then a second and last around the first axis again. The Tait-Bryan angles is similar to the Euler angles with the difference that they express rotation around all three axis.
A problem with Euler and Tait-Bryan angles is that if the coordinate system is rotated 90 ° in pitch, the x- and z-axis will align. This causes rotations around x to be the same as rotations around z meaning that one degree of freedom is lost [23]. This problem is called gimbal lock and has to be considered when using Euler or Tait-Bryan angles.

2.3.2 Rotation matrices

To rotate a vector in one coordinate system to another, rotation matrices is a well established method often used in IMU contexts. Rotation matrices are used to rotate a vector by an angle

$$\mathbf{\Theta} = \begin{bmatrix} \theta \\ \varphi \\ \psi \end{bmatrix} \tag{2.6}$$

without changing the length of the vector. In two dimensions rotations around x,y,z, denoted $\mathbf{\Theta}$ can be expressed as the rotation matrices

$$R_x(\theta) = \begin{bmatrix} 1 & 0 & 0 \\ 0 & c(\theta) & -s(\theta) \\ 0 & s(\theta) & c(\theta) \end{bmatrix}, \quad R_y(\varphi) = \begin{bmatrix} c(\varphi) & 0 & s(\varphi) \\ 0 & 1 & 0 \\ -s(\varphi) & 0 & c(\varphi) \end{bmatrix}, \quad R_z(\psi) = \begin{bmatrix} c(\psi) & -s(\psi) & 0 \\ s(\psi) & c(\psi) & 0 \\ 0 & 0 & 1 \end{bmatrix}. \tag{2.7}$$

A rotation can be performed by multiplying a vector around one axis at the time but a more compact solution is to multiply the vector with a matrix describing the full three dimensional rotation. This matrix is called a direct cosine matrix (DCM) [6] and is defined as (in Tait-Bryan angles)

$$R(\theta,\varphi,\psi) = R_z(\psi)R_y(\varphi)R_x(\theta) \tag{2.8}$$

or equivalently

$$R = \begin{bmatrix} c(\theta)c(\psi) & s(\theta)s(\varphi)c(\psi) - c(\theta)s(\psi) & c(\theta)s(\varphi)c(\psi) + s(\theta)s(\psi) \\ c(\theta)s(\psi) & s(\theta)s(\varphi)s(\psi) + c(\theta)c(\psi) & c(\theta)s(\varphi)s(\psi) - s(\theta)c(\psi) \\ -s(\theta) & s(\theta)c(\varphi) & c(\theta)c(\varphi) \end{bmatrix}. \tag{2.9}$$

Since $R(\theta,\varphi,\psi)$ is only describing a rotation it is in fact another way to describe the orientation in terms of unit vectors. To rotate a vector $\mathbf{v}$ by (θ,φ,ψ) in 3D-space the DCM is used as

$$\mathbf{v}' = R(\theta,\varphi,\psi)\mathbf{v}, \tag{2.10}$$

where $\mathbf{v}'$ is the rotated vector. DCM are often used to transform vectors from a sensor frame S to a global earth frame NED, especially in IMU areas where the interesting orientation is often the one relative the earth or a room. This would mean that using angular information the sensor frame vector $\mathbf{v}^S$ can be expressed in earth frame NED as

$$\mathbf{v}^{NED} = R(\theta,\varphi,\psi)\mathbf{v}^S. \tag{2.11}$$

To rotate a vector from NED to S the inverse of $R(\theta,\varphi,\psi)$ is used as

$$\mathbf{v}^S = (R(\theta,\varphi,\psi))^{-1}\mathbf{v}^{NED} \tag{2.12}$$

and because $R(\theta,\varphi,\psi)$ is an orthogonal matrix

$$(R(\theta,\varphi,\psi))^{-1} = (R(\theta,\varphi,\psi))^T. \tag{2.13}$$

2.3.3 Quaternion representation

A common way to describe rotations is to use Euler or Tait-Bryan angles, but as explained earlier this is not suitable in practical applications due to the risk of gimbal lock. Another way of expressing is to use quaternions, this is a method mainly used to gain computational efficiency [24]. This comes from the fact that quaternion rotation needs

less multiplications. The quaternion representation has also an advantage that it does not suffer from gimbal lock. A quaternion is a four-dimensional complex number that can be used to describe a coordinate system S relative another coordinate system NED. This can be described in three dimensions as a rotation of S around a unit vector $\mathbf{r}$ with an angle of θ. This rotation is shown in Figure 2.3.

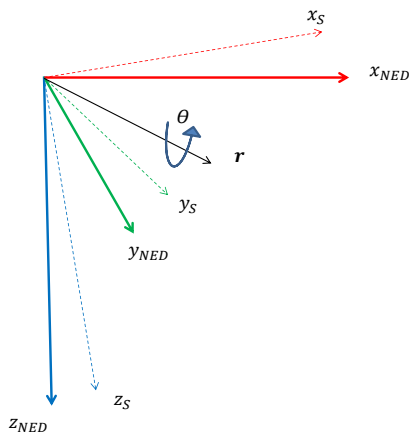

Figure 2.3: Rotation of a coordinate system around a unit vector.

This gives the quaternion expressing the sensor frame S's orientation relative NED as

$$\mathbf{q} = \begin{bmatrix} q_0 \\ q_1 \\ q_2 \\ q_3 \end{bmatrix} = \begin{bmatrix} \cos(\frac{\theta}{2}) \\ -r_x \sin(\frac{\theta}{2}) \\ -r_y \sin(\frac{\theta}{2}) \\ -r_z \sin(\frac{\theta}{2}) \end{bmatrix}. \tag{2.14}$$

To use quaternion for rotation it is necessary to understand a concept called quaternion product. The quaternion product between two quaternions a and b is defined as [9]

$$\mathbf{a} \otimes \mathbf{b} = \begin{bmatrix} a_1b_1 - a_2b_2 - a_3b_3 - a_4b_4 \\ a_1b_2 + a_2b_1 + a_3b_4 - a_4b_3 \\ a_1b_3 - a_2b_4 + a_3b_1 + a_4b_2 \\ a_1b_4 + a_2b_3 - a_3b_2 + a_4b_1 \end{bmatrix} \tag{2.15}$$

and can be used to express compound orientation. A vector $\mathbf{v}^S$ in S can be expressed in NED by rotating it with the quaternion [9]

$$\mathbf{v}^S = \mathbf{q} \otimes \mathbf{v}^{NED} \otimes \mathbf{q}^* \tag{2.16}$$

where $\mathbf{q}^*$ is the conjugate of the quaternion. This corresponds to using a DCM rotation matrix as explained earlier and in quaternion notation the rotation matrix can be expressed as

$$Q(\mathbf{q}) = \begin{bmatrix} 2q_0^2 - 1 + 2q_1^2 & 2q_1q_2 - 2q_0q_3 & 2q_1q_3 + 2q_0q_2 \\ 2q_1q_2 + 2q_0q_3 & 2q_0^2 - 1 + 2q_2^2 & 2q_2q_3 - 2q_0q_1 \\ 2q_1q_3 - 2q_0q_2 & 2q_2q_3 + 2q_0q_1 & 2q_0^2 - 1 + 2q_3^2 \end{bmatrix} \tag{2.17}$$

which means that the rotation of $\mathbf{v}^S$ to NED can be accomplished by

$$\mathbf{v}^{NED} = Q(\mathbf{q})\mathbf{v}^S \tag{2.18}$$

To express orientation gyroscopic sensors are often used. The measurements from the sensor can be considered as a vector containing x,y,z components of the angular rate, and by inserting a 0 as the first vector element to get four dimensions the angular rate vector can be written as

$$\omega = \begin{bmatrix} 0 \\ \omega_x \\ \omega_y \\ \omega_z \end{bmatrix} \tag{2.19}$$

The measurements from the sensor are expressed in the sensor frame and needs to be rotated to the NED frame. This is done using (2.16), but since the vector to be rotated contains the derivative of the orientation, the quaternion expression needs to be differentiated [25] as

$$\dot{\mathbf{q}} = \frac{1}{2}\mathbf{q} \otimes \omega = \frac{1}{2} \begin{bmatrix} 0 & -\omega_x & -\omega_y & \omega_z \\ \omega_x & 0 & \omega_x & -\omega_y \\ \omega_y & -\omega_z & 0 & \omega_x \\ \omega_z & \omega_y & -\omega_x & 0 \end{bmatrix} \mathbf{q}. \tag{2.20}$$

By simply integrating (2.20)

$$\mathbf{q}_k = \mathbf{q}_{k-1} + \dot{\mathbf{q}}_k T_s \tag{2.21}$$

the orientation of the sensor expressed in quaternions is obtained.

For more intuitive visualizations the quaternions are often converted to Euler angles in roll, pitch and heading as [6]

$$\theta = atan2(\frac{2q_2q_3 + 2q_0q_1}{2q_0^2 + 2q_3^2 - 1}) \tag{2.22}$$

$$\varphi = -asin(2q_2q_3 - 2q_0q_2) \tag{2.23}$$

$$\psi = atan2(\frac{2q_1q_2 + 2q_0q_3}{2q_0^2 + 2q_1^2 - 1}) \tag{2.24}$$

2.4 Sensor fusion

Sensor fusion is a term that in recent years has become popular in all types of applications using sensors. As the name implies the term describes usage of more than one sensor fused together to improve measurements. The basic idea is that several sensors used together can be better than each sensor individually. This section describes typical model based sensor fusion algorithms.

2.4.1 State space models

State space models are a useful way of describing how a system behaves. The base of this type of model is a state vector describing the current state of the system, a motion model describing how these states are expected to change between times and a measurement model that describes the output in terms of the state vector.

Motion model

The motion model describe how the states propagate in time.

$$\mathbf{x}_{k+1} = F_k\mathbf{x}_k + \boldsymbol{\delta}_k \tag{2.25}$$

where $\boldsymbol{\delta}_k$ is normally distributed process noise

$$\boldsymbol{\delta}_k \sim \mathcal{N}(\mathbf{0},D_k) \tag{2.26}$$

The process noise is a parameter that tells how much the states are expected to move between instances of time. Another way of representing the motion model assuming that it is a Gauss-Markov model [26] is by denote it as a probability distribution

$$p(\mathbf{x}_k|x_{k-1}) = \mathcal{N}(\mathbf{x}_k|F_{k-1}\mathbf{x}_{k-1},D_k), \tag{2.27}$$

where $F_{k-1}\mathbf{x}_{k-1}$ is the expected value and D_k is the covariance. This representation will be used later to describe the Kalman filter.

Motion models are often adapted to the type of motion that is estimated. The idea is that if there is some extra knowledge on how the states are propagating this can improve filter estimates. There are several standard models that can be used and the simplest of all are the random walk model. Basically what the random walk model says is that there is no knowledge of how the next state is going to be. The only constraint is how far the state can move between instances of time while the direction is arbitrary. This constraint is expressed in the process noise that describes how much from the current state the next state should be. Using equation (2.25) the random walk model would look like

$$\mathbf{x}_{k+1} = \mathbf{x}_k + \boldsymbol{\delta}_k \tag{2.28}$$

with normally distributed process noise

$$\boldsymbol{\delta}_k \sim \mathcal{N}(\mathbf{0},D_k) \tag{2.29}$$

This means that the next state is just the last state with some added movement determined by the process noise, and this is a very generalized model.

Measurement model

The states in the model do not have to be in the same domain as the measurements. But to compare the measurements with the states, the states must be mapped to the same domain as the measurements. The model describing this mapping is called a measurement model and is expressed as

$$\mathbf{y}_k = H_k \mathbf{x}_k + \boldsymbol{\varepsilon}_k \tag{2.30}$$

where H_k is a matrix mapping the states to the same domain as the measurements, and the measurement noise

$$\boldsymbol{\varepsilon}_k \sim \mathcal{N}(\mathbf{0}, E_k) \tag{2.31}$$

or as in the form of probability distribution [26]

$$p(\mathbf{y}_k|\mathbf{x}_k) = \mathcal{N}(\mathbf{x}_k|H_k\mathbf{x}_k, E_k). \tag{2.32}$$

The measurement noise is just as the process noise assumed to be white Gaussian distributed and describes how noisy the measurements are expected to be. In a practical application the measurement noise describes how noisy a sensor is described by the random walk and this can easily be measured by observing the sensor output when it is not excited.

2.4.2 Kalman filter

The Kalman filter is the most common method for sensor fusion and is an algorithm based on linear models of dynamics and minimizes the uncertainties of the states. It is used to estimate the states in the state vector using measurements affected by noise and/or other inaccuracies. The Kalman filter is a recursive filter that for each instance of time predicts the next state given a model of dynamics and updates the current state using the prediction and measurements. These steps are referred to as the prediction step and the update step. By using the probability distribution notation and that the posterior distribution is calculated recursively, the distribution for the previous step can be assumed to be Gaussian as

$$p(\mathbf{x}_{k-1}|\mathbf{y}_{1:k-1}) = \mathcal{N}(x_{k-1}|\hat{\mathbf{x}}_{k-1}, P_{k-1}) \tag{2.33}$$

It can then be shown that the predicted distribution of the states given the measurements up to time $k-1$ can be expressed as [27]

$$p(\mathbf{x}_k|\mathbf{y}_{1:k-1}) = \mathcal{N}(\mathbf{x}_k|F_{k-1}\hat{\mathbf{x}}_{k-1}, F_{k-1}P_{k-1}F_{k-1}^T + D_k). \tag{2.34}$$

This corresponds to the prediction step where the expected value is the predicted state

$$\hat{\mathbf{x}}_{k|k-1} = F_k \hat{\mathbf{x}}_{k-1|k-1} \tag{2.35}$$

and the predicted state covariance

$$P_{k|k-1} = F_k P_{k-1|k-1} F_k^T + D_k. \tag{2.36}$$

In a similar way the update step can be derived according to [27] as the distribution

$$p(\mathbf{x}_k|\mathbf{y}_k) = \mathcal{N}(\mathbf{x}_k|\hat{\mathbf{x}}_k, P_k) \tag{2.37}$$

with the expected value

$$\hat{\mathbf{x}}_{k|k} = \hat{\mathbf{x}}_{k|k-1} + K_k \mathbf{v}_k \tag{2.38}$$

and covariance

$$P_{k|k} = P_{k|k-1} - K_k S_k K_k^T. \tag{2.39}$$

Here v_k denotes the innovation

$$\mathbf{v}_k = \mathbf{y}_k - H_k \hat{\mathbf{x}}_{k|k-1}, \tag{2.40}$$

and S_k the innovation covariance that tells how confident we are in that the measurements are correct

$$S_k = H_k P_{k|k-1} H_k^T + E_k. \tag{2.41}$$

The Kalman gain K_k

$$K_k = P_{k|k-1} H_k S_k^{-1} \tag{2.42}$$

is used to determine how much from the innovation the prediction should be corrected with.

2.4.3 Extended Kalman filter

The Kalman filter is based on linear motion and measurement models, however these models often suffer from nonlinearities. An arbitrary nonlinear state space model can be expressed as functions of the state vector. The motion model is then expressed as

$$\mathbf{x}_{k+1} = f(\mathbf{x}_k) + \boldsymbol{\delta}_k \tag{2.43}$$

and the nonlinear measurement model

$$\mathbf{y}_k = h(\mathbf{x}_k) + \boldsymbol{\varepsilon}_k \tag{2.44}$$

This means that the Kalman filter needs to be modified to handle the nonlinear situations. The Extended Kalman Filter (EKF) is linearizing the models for each recursion of time and uses the linearized models in the Kalman filter. Basically the EKF follows the same algorithm as the Kalman filter but with the linearized models f' and h' instead of F and H as in the regular Kalman filter. [28] The prediction step for the states then becomes

$$\hat{\mathbf{x}}_{k|k-1} = f(\hat{\mathbf{x}}_{k-1|k-1}) \tag{2.45}$$

and the predicted covariance matrix is calculated with the linearized transition matrix as

$$P_{k|k-1} = f'(\hat{\mathbf{x}}_{k-1|k-1})P_{k-1|k-1}f'(\hat{\mathbf{x}}_{k-1|k-1})^T + D_k. \tag{2.46}$$

And the update step can then be formed as

$$S_k = h'(\hat{\mathbf{x}}_{k|k-1})P_{k|k-1}h'(\hat{\mathbf{x}}_{k|k-1})^T + E_k, \tag{2.47}$$

$$K_k = P_{k|k-1}h'(\hat{\mathbf{x}}_{k|k-1})^T S_k^{-1}, \tag{2.48}$$

$$\hat{\mathbf{x}}_{k|k} = \hat{\mathbf{x}}_{k|k-1} - K_k(\mathbf{y}_k - h(\hat{\mathbf{x}}_{k|k-1})). \tag{2.49}$$

2.4.4 Quaternion based orientation filter, QEKF

A simple general filter for expressing orientation in terms of quaternions using gyroscopes and accelerometers is designed in [25]. The quaternions are chosen for state vector as

$$\hat{\mathbf{x}}_k = \begin{bmatrix} q_0 \\ q_1 \\ q_2 \\ q_3 \end{bmatrix} \tag{2.50}$$

In this filter the gyroscope signal with sample time T_s is assumed to be good enough to use as an input signal

$$\hat{\mathbf{x}}_{k+1} = (I + \frac{1}{2}S(\omega_k)T_s)\mathbf{x}_k + \frac{T_s}{2}\bar{S}(\mathbf{x}_k)\varepsilon_k^{gyr} \tag{2.51}$$

with

$$\bar{S}(\omega_k) = \begin{bmatrix} 0 & -\omega_x & -\omega_y & \omega_z \\ \omega_x & 0 & \omega_x & -\omega_y \\ \omega_y & -\omega_z & 0 & \omega_x \\ \omega_z & \omega_y & -\omega_x & 0 \end{bmatrix} \quad S(\mathbf{x}_k) = \begin{bmatrix} -q_1 & -q_2 & -q_3 \\ q_0 & -q_3 & q_2 \\ q_3 & q_0 & -q_1 \\ -q_2 & q_1 & q_0 \end{bmatrix} \tag{2.52}$$

This model is used in the Kalman prediction step described in (2.45)-(2.46) with

$$f(\mathbf{x}_k) = (I + \frac{1}{2}S(\omega_k)T_s)\mathbf{x}_k \tag{2.53}$$

and the process noise covariance matrix is defined in terms of the current states and the measurement noise covariance matrix as

$$D_k = (\frac{T_s}{2}\bar{S}(\mathbf{x}_k))E^{gyr}(\frac{T_s}{2}\bar{S}(\mathbf{x}_k))^T. \tag{2.54}$$

The measurement model for the accelerometer is defined as

$$\mathbf{y}_k^{acc} = Q^T(\mathbf{x}_k)(\mathbf{g}^0 + \mathbf{f}_k^t) + \varepsilon_k^{acc} \tag{2.55}$$

which is used to find the attitude of the sensor. $\mathbf{g}^0$ is here the nominal gravity vector which is assumed to be constant. $\mathbf{f}_k^{acc}$ is external forces due to accelerations in translational directions. In this filter $\mathbf{f}_k^t$ is considered small enough to be neglected causing the model to be valid for pure rotations of the sensor. The measurement model for the accelerometer is nonlinear which means that the extended Kalman filter needs to be used and in this case the function that is linearized is

$$h(\mathbf{x}_k) = Q^T(\mathbf{x}_k)\mathbf{g}^0 \tag{2.56}$$

With the linearized measurement function $h'(\mathbf{x}_k)$ the EKF update step is implemented according to equations (2.47)-(2.49) and the filter is estimating the orientation. However since the filter is not using magnetometer inputs the heading is not accurately estimated. The only information the filter has in heading is from the gyroscope signal and that can only describe relative rotation.

2.5 Linear combiners

The term linear combiner is referring to the technique of combining parts of a signal to produce the signal itself. This can be useful when working with periodic signals that can be built by harmonics and amplitudes. In this section a certain type of linear combiners is introduced, these linear combiners can be used as adaptive filters if there is some idea of the shape of the signal that is being tracked. These linear combiners are called Fourier linear combiners.

2.5.1 Fourier linear combiner

Fourier linear combiner (FLC) is a method for tracking a periodic signal. The method is derived from the Fourier series where every periodic signal can be written as a sum of sine waves as

$$\mathbf{y}_k = \sum_{r=1}^{M} a_{r_k} \sin(r\omega_0 k) + b_{r_k} \cos(r\omega_0 k). \tag{2.57}$$

This is a linear representation of the nonlinear amplitude-phase representation

$$\mathbf{y}_k = A_k \sin(\omega k + \phi_k) \tag{2.58}$$

and it can be shown [29] that

$$A_k = \sqrt{a_k^2 + b_k^2} \tag{2.59}$$

$$\phi_k = \arctan(\frac{a_k}{b_k}) \tag{2.60}$$

For the FLC the fundamental frequency ω_0 is fixed and the amplitude weights a_r and b_r are unknown. What the FLC does is that it uses an extension of the LMS filter to

calculate a_r and b_r as adaptive gains

$$\mathbf{w}_k = \begin{bmatrix} a_{1k} \\ \vdots \\ a_{Mk} \\ b_{(M+1)k} \\ \vdots \\ b_{2Mk} \end{bmatrix} \tag{2.61}$$

that is used together with a matrix

$$H_{rk} = \begin{cases} \sin(rT_s \sum_{j=0}^{k} \omega_{0_j}), & 1 \leq r \leq M \\ \cos(rT_s \sum_{j=0}^{k} \omega_{0_j}), & M+1 \leq r \leq 2M \end{cases} \tag{2.62}$$

describing the sinusoidal parts of the signal. The error to be minimized is defined as

$$e_k = \mathbf{y}_k - H_k \mathbf{w}_k \tag{2.63}$$

where $H_k \mathbf{w}_k$ is the reconstructed signal. The LMS-algorithm computes the adaptive gains by minimizing e_k [30] as

$$\mathbf{w}_{k+1} = \mathbf{w}_k + 2\mu e_k H_k \tag{2.64}$$

The concept of the FLC algorithm is illustrated as a block chart in Figure 2.4.

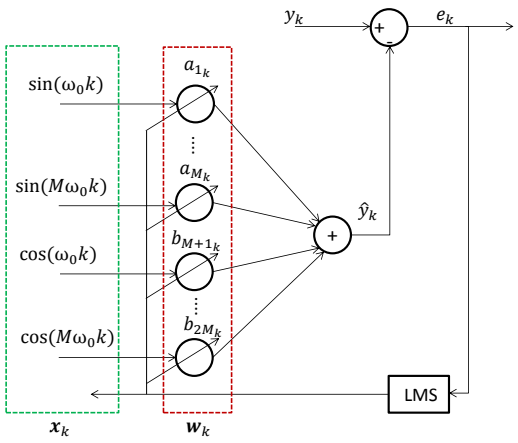

Figure 2.4: Illustrative explanation of the FLC algorithm.

2.5.2 BMFLC

A more effective method originating from FLC is the Bandlimited multiple FLC (BMFLC) [12]. The main concept of this filter is to assume that the approximate frequencies present in the signal that is tracked are known. This gives the possibility to specify a list of frequencies $\begin{bmatrix}\omega_1 & \cdots & \omega_n\end{bmatrix}$ where the frequency of the motion is located. This approach makes it possible to track more than one dominant frequency and makes the adaptation faster for sudden changes in frequency [12]. In the same sense as in FLC the sinusoidal terms are ordered in a vector but now with one term per frequency component

$$H_k = \begin{bmatrix}\sin(\omega_1 k) & \sin(\omega_2 k) & \cdots & \sin(\omega_n k) \\ \cos(\omega_1 k) & \cos(\omega_2 k) & \cdots & \cos(\omega_n k)\end{bmatrix} \tag{2.65}$$

The weight vector is now limited to a set of frequencies and can be written as

$$\mathbf{w}_k = \begin{bmatrix}\begin{bmatrix}a_{1k} & a_{2k} & \cdots & a_{nk}\end{bmatrix}^T \\ \begin{bmatrix}b_{1k} & b_{2k} & \cdots & b_{nk}\end{bmatrix}^T\end{bmatrix} \tag{2.66}$$

and the estimated signal can be built in the same way as in the FLC case as

$$\hat{\mathbf{y}}_k = H_k \mathbf{w}_k. \tag{2.67}$$

The BMFLC is explained illustratively in Figure 2.5 and it is clear that the only difference from FLC is that more frequencies are used

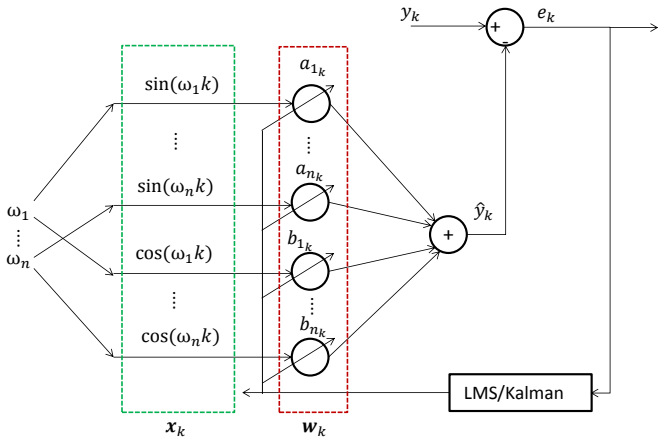

Figure 2.5: Illustrative explanation of the BMFLC algorithm.

Instead of using LMS one could use Kalman filtering as explained in Section 2.4.2 to estimate the amplitudes $\mathbf{w}_k$. This would mean that the matrix H_k corresponds to the measurement matrix.

3

MATHEMATICAL MODELS AND FILTER DESIGN

The following chapter explains the typical motion of the investigated radar platform which motivates the developed filter design. The motion also motivates the mathematical models used in the Kalman based design divided in two parts, one describing the short term dynamics and one the second the long term dynamics. The modeling takes into account available sensor data and error parameters such as bias and high frequent noise.

3.1 System motion behaviour (Periodic motion)

To be able to design a model based filter for the inertial sensor mounted on the radar system we first need to analyse the type of motion that characterizes its behaviour. A log of the orientation from the reference system discussed in Section 1.5 is shown in Figure 3.1. During the log the radar antenna rotates at 60 rpm and it is the behaviour during this condition that will serve as a foundation for characterizing the behaviour of the system.

As seen from Figure 3.1 there are two elements that make up the variation of the orientation over time, the short term dynamics and the long term. In a time window of 10 seconds as in Figure 3.1b the roll and pitch appears to move periodically with a constant frequency. The heading does on the other hand not appear to have any dominating behaviour that can be expressed as any trivial mathematical function.

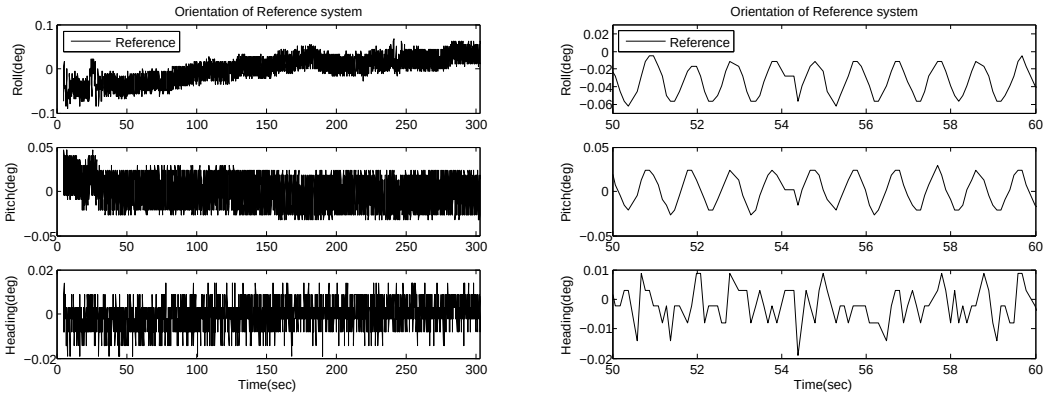

(a) Reference motion **(b)** Zoomed in on 10 seconds of data.

Figure 3.1: Recorded motion of the reference system.

The roll and pitch behaviour over a longer period of time (300 sec.) as in Figure 3.1a can be seen as more of a drifting motion that changes relatively slow and without any clear trajectory or trend. As to what to conclude about the heading there is no obvious model that fits is movement, at least not with the provided resolution given by the reference.

Both the short and long term dynamical behaviour is consistent with what can be expected of the radar platform upon which the reference system is mounted. To elaborate on this the short term periodical behaviour in roll and pitch can be motivated by the rotating radar antenna likely being not perfectly balanced, which explains why the pattern appears time after time and also coincides with the antennas rotational rate of 60 rpm. Why this periodic behaviour is not seen in the heading can be attributed to that the mast that the radar antenna is mounted on is much stiffer with regards to twisting along its axis, which would need to occur on order for the heading to change.

The observed long term dynamics would ideally be a constant angle seeing as the scenario being evaluated for the radar system is that it is deployed as a stationary outpost and not moving during the evaluation. But the movement can have a stationary orientation that varies slightly over time since the radar system rests on the suspension of a truck and is not directly constrained by any supporting struts.

3.2 Filter design, the periodic filter

The following sections will focus on the formulation of mathematical models. The radar system's orientation is represented by the column vector

$$\mathbf{\Theta} = \begin{bmatrix} \theta \\ \varphi \\ \psi \end{bmatrix} \tag{3.1}$$

where θ, φ, ψ denotes roll, pitch and heading respectively. The platform orientation can, as stated in Section 3.1, be described as periodic to some extent. The orientation is however not a periodic signal centred about a constant level but can rather be decomposed into two parts or what further on will be called components. The first component is the periodic which has relatively fast dynamics and oscillates around the other component which has considerably slower and less predictable dynamics. This slower component can be considered as the stationary level of the orientation which also relates the periodic component to the global NED orientation frame.

By denoting the periodic component as Θ^p and the stationary component as Θ^s we can formulate the decomposition of the complete orientation Θ as the sum of the two components according to

$$\mathbf{\Theta} = \mathbf{\Theta}^p + \mathbf{\Theta}^s. \tag{3.2}$$

Because of this decomposition each of the two components will need to be estimated in order to estimate the complete orientation $\mathbf{\Theta}$.

Since the component $\mathbf{\Theta}^p$ is an angle and possess periodic properties it by extension also means that its derivative, or the angular rate as it also may be referred to, also will be periodic. The angular rate of the orientation can be measured by a gyroscope and the BMFLC-Kalman filter explained in Section 2.5.2 is a filter which is designed to take advantage of periodic signal properties. The resulting estimate from the filter becomes an estimate of the derivative of the periodic component $\mathbf{\Theta}^p$ which then can be integrated to estimate the actual angles. This argument serves as motivation as to why it is suitable to use a BMFLC-Kalman filter with angular rates from a gyroscope as input in order to estimate the periodic component $\mathbf{\Theta}^p$.

To estimate the stationary component $\mathbf{\Theta}^s$ there is a need to describe the orientation of the sensor in relation to the global NED frame. Seeing as gravity is a constant force present in both the sensor frame and the NED frame, and which also can be measured by an accelerometer, it can be used to estimate the stationary component $\mathbf{\Theta}^s$. A common filter design used for estimation orientation given measurements of gravity is an EKF similar to that explained in [25].

The filters proposed to estimate the periodic component $\mathbf{\Theta}^p$ and stationary component $\mathbf{\Theta}^s$ can be presented as parts of a larger filter design which estimates the complete orientation. This complete design can be represented as a block diagram which is seen in Figure 3.2.

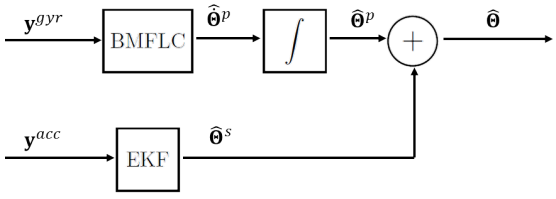

Figure 3.2: Block diagram of the periodic filter.

Both the periodic and stationary component filters are based upon the Kalman filter

and will in the following sections be explained separately from one another. Each section will first motivate a state vector for each of the components before moving on to state motion models and how they are used to formulate the prediction step of the Kalman filter algorithm. Finally the filter descriptions explains the states measurement models used for the Kalman algorithms measurement update step along with any eventual observation model needed for the estimate which concludes the complete filter descriptions.

3.2.1 Periodic orientation component estimation

The BMFLC filter works under assumption that the signal to be estimated (roll, pitch and heading rates) can be constructed from a known and finite number of constant periodic frequencies. The signals in this filter design each have their own set of these constant frequencies defined as

$$\omega^{\theta} = \begin{bmatrix} \omega_1^{\theta} \\ \vdots \\ \omega_{\varsigma}^{\theta} \end{bmatrix}, \quad \omega^{\varphi} = \begin{bmatrix} \omega_1^{\varphi} \\ \vdots \\ \omega_{\tau}^{\varphi} \end{bmatrix}, \quad \omega^{\psi} = \begin{bmatrix} \omega_1^{\psi} \\ \vdots \\ \omega_{\upsilon}^{\psi} \end{bmatrix}, \tag{3.3}$$

where ς,τ and υ are the corresponding number of frequencies for each signal. By selecting these frequencies we determine what in the input signal the desired information is and should be included in the estimated signal output. To motivate the selection of which frequencies to include we can analyze the frequency content of the input signal using Fast Fourier transform (FFT). The FFT will indicate the frequency of any present periodic signals, as the desired angular rate, within the input signal but also any noise, bias and variation of the stationary orientation component $\mathbf{\Theta}^s$. The noise is however assumed to be spread out evenly over the frequency spectrum of the FFT and the bias and variation of the stationary orientation component $\mathbf{\Theta}^s$ as a frequency very close to 0 Hz as they are assumed to change very slowly over time. By disregarding the frequencies associated with noise and low frequencies all that are left are the periodic frequencies of the desired angular rates. From Figure 3.1 we can observe that the roll and pitch are likely to have a single dominating frequency and the selection of frequencies for roll and pitch can with this in mind be made as a narrow band of frequencies covering the dominating frequency to increase the robustness in case the periodic frequency should vary. The angular rate of the heading is however more likely to contain several frequencies. As the number of frequencies affect the size of the BMFLC state vector it can therefore be wiser to select only the actual dominating periodic frequencies as opposed to a range covering each of them. Since the an increase in the size of the state vector increases the computational requirement of the filter the more sparse selection suggested for heading offers a more computationally efficient selection for several dominating frequencies spread out over a wider range.

For each one of the selected frequencies there are two associated coefficients for the odd and even terms of the frequency according to the Fourier decomposition of periodic signals [29]. The odd and even Fourier coefficients are denoted $\mathbf{a}$ and $\mathbf{b}$ and

by extending the BMFLC state vector with states to estimate any existing bias of the gyroscope measurements the final state vector can be described as

$$\mathbf{x}^p = \begin{bmatrix} \mathbf{a}^\theta & \mathbf{b}^\theta & \mathbf{a}^\varphi & \mathbf{b}^\varphi & \mathbf{a}^\psi & \mathbf{b}^\psi & \mu^{gyr_\theta} & \mu^{gyr_\varphi} & \mu^{gyr_\psi} \end{bmatrix}^T \tag{3.4}$$

where

$$\mathbf{a}^\theta = \begin{bmatrix} a_1^\theta \\ \vdots \\ a_\varsigma^\theta \end{bmatrix}^T, \mathbf{b}^\theta = \begin{bmatrix} b_1^\theta \\ \vdots \\ b_\varsigma^\theta \end{bmatrix}^T, \quad \mathbf{a}^\varphi = \begin{bmatrix} a_1^\varphi \\ \vdots \\ a_\tau^\varphi \end{bmatrix}^T, \mathbf{b}^\varphi = \begin{bmatrix} b_1^\varphi \\ \vdots \\ b_\tau^\varphi \end{bmatrix}^T, \quad \mathbf{a}^\psi = \begin{bmatrix} a_1^\psi \\ \vdots \\ a_\upsilon^\psi \end{bmatrix}^T, \mathbf{b}^\psi = \begin{bmatrix} b_1^\psi \\ \vdots \\ b_\upsilon^\psi \end{bmatrix}^T. \tag{3.5}$$

Since the input to the filter relates to the derivative of the periodic component Θ^p, as opposed to measuring the actual angles of the components, the resulting estimates will need to be integrated. A trivial solution to this would be to add the integrated states as for the states in the state vector and integrate them by means of numeric integration. Numeric integration is however problematic due to that any errors in the derivative domain will cause the integrated estimate to drift over time making its errors theoretically unbounded. The BMFLC-Kalman filter offers unique capabilities in terms of performing integration since the state vector actually describes the properties of a constant periodic signal rather an estimate of the single sample of the measured signal. These periodic properties is of great value when performing integration since it means that the signal can be analytically integrated as opposed to the numerical method. Exactly how this analytic integration is performed will be explained in detail further on but for now it is enough to know that the chosen state vector can be used to fully describe the periodic component $\mathbf{\Theta}^p$ in terms of angles as well as angular rates.

State motion model and filter prediction

The Fourier coefficients and biases in the state vector (3.4) are assumed to change according to a random walk behaviour. This results in a state space model which describes the state dynamics as

$$\mathbf{x}_{k+1}^p = F^p \mathbf{x}_k^p + \boldsymbol{\delta}_k^p \tag{3.6}$$

$$\boldsymbol{\delta}_k^p \sim \mathcal{N}(\mathbf{0}, D_k^p), \tag{3.7}$$

where F^p is the state transition matrix defined as

$$F^p = I_{2(\varsigma+\tau+\upsilon)+3}. \tag{3.8}$$

By using the modified Euler method as described in [31] the process noise covariance matrix D_k^p can be selected as

$$D_k^p = T_s \tilde{D}^p \tag{3.9}$$

where T_s is the sampling time.

The prediction step of the BMFLC-Kalman filter at time k can now be described by the algorithm

$$\hat{\mathbf{x}}_{k|k-1}^p = F^p \hat{\mathbf{x}}_{k-1|k-1}^p \tag{3.10}$$

$$P_{k|k-1}^p = F^p P_{k-1|k-1}^p (F^p)^T + D_k^p. \tag{3.11}$$

State measurement model and filter update

Any constant level apart from the true rotation in the gyroscope measurement can be seen as a bias since the radar system is stationary. This leads to that the measured angular rates from the gyroscope can be modelled using the relation

$$\mathbf{y}_k^{gyr} = \underbrace{\begin{bmatrix} (\sum_{i=1}^{\varsigma} a_{ik}^{\theta} \sin(\omega_i^{\theta} k) + b_{ik}^{\theta} \cos(\omega_i^{\theta} k)) \\ (\sum_{i=1}^{\tau} a_{ik}^{\varphi} \sin(\omega_i^{\varphi} k) + b_{ik}^{\varphi} \cos(\omega_i^{\varphi} k)) \\ (\sum_{i=1}^{\upsilon} a_{ik}^{\psi} \sin(\omega_i^{\psi} k) + b_{ik}^{\psi} \cos(\omega_i^{\psi} k)) \end{bmatrix}}_{\dot{\mathbf{\Theta}}_k^p} + \begin{bmatrix} \mu^{gyr_\theta} \\ \mu^{gyr_\varphi} \\ \mu^{gyr_\psi} \end{bmatrix} + \boldsymbol{\varepsilon}_k^{gyr} \tag{3.12}$$

$$\boldsymbol{\varepsilon}_k^{gyr} \sim \mathcal{N}(\mathbf{0}, E_k^{gyr}). \tag{3.13}$$

This can be translated into the *linear* state space measurement model

$$\mathbf{y}_k^{gyr} = H_k^p \mathbf{x}_k^p + \boldsymbol{\varepsilon}_k^{gyr} \tag{3.14}$$

where H_k^p is the measurement matrix at time k defined by

$$H_k^p = \begin{bmatrix} \mathbf{h}_k^{\theta} & \mathbf{0} & \mathbf{0} & 1 & 0 & 0 \\ \mathbf{0} & \mathbf{h}_k^{\varphi} & \mathbf{0} & 0 & 1 & 0 \\ \mathbf{0} & \mathbf{0} & \mathbf{h}_k^{\psi} & 0 & 0 & 1 \end{bmatrix} \tag{3.15}$$

in which

$$\mathbf{h}_k^{\theta} = \begin{bmatrix} \sin(\omega_1^{\theta} k) & \cdots & \sin(\omega_{\varsigma}^{\theta} k) & \cos(\omega_1^{\theta} k) & \cdots & \cos(\omega_{\varsigma}^{\theta} k) \end{bmatrix} \tag{3.16}$$

$$\mathbf{h}_k^{\varphi} = \begin{bmatrix} \sin(\omega_1^{\varphi} k) & \cdots & \sin(\omega_{\tau}^{\varphi} k) & \cos(\omega_1^{\varphi} k) & \cdots & \cos(\omega_{\tau}^{\varphi} k) \end{bmatrix} \tag{3.17}$$

$$\mathbf{h}_k^{\psi} = \begin{bmatrix} \sin(\omega_1^{\psi} k) & \cdots & \sin(\omega_{\upsilon}^{\psi} k) & \cos(\omega_1^{\psi} k) & \cdots & \cos(\omega_{\upsilon}^{\psi} k) \end{bmatrix}. \tag{3.18}$$

It can be noted that the measurement matrix H_k^p is *linear* with respect to the state vector even if it is not linear with respect to time.

The innovation and the BMFLC-Kalman gain K_k^p can now be calculated according to

$$\mathbf{v}_k^p = \mathbf{y}_k^{gyr} - H_k^p \hat{\mathbf{x}}_{k|k-1}^p \tag{3.19}$$

$$S_k^p = H_k^p P_{k|k-1}^p (H_k^p)^T + R_k^p \tag{3.20}$$

$$K_k^p = P_{k|k-1}^p H_k^p (S_k^p)^{-1} \tag{3.21}$$

and the measurement update at time k is then described by

$$\hat{\mathbf{x}}_{k|k}^p = \hat{\mathbf{x}}_{k|k-1}^p + K_k^p \mathbf{v}_k^p \tag{3.22}$$

$$P_{k|k}^p = P_{k|k-1}^p - K_k^p S_k^p (K_k^p)^T \tag{3.23}$$

Analytic integration of the periodic orientation rate

The estimated states and measurement model have up to this point only been described as an abstract representation relating to the periodic orientation component's angular rate $\dot{\mathbf{\Theta}}^p$. But since the periodic filter is intended to estimate an angle as its output there is a need to relate the states to the desired angular domain as opposed to its derivative domain. To formulate the relation between the state vector $\mathbf{x}^p$ and the angles in the periodic orientation component $\mathbf{\Theta}^p$ we can utilize a method similar to that described in [12]. The method takes advantage of the fact that the periodic component's angular rate $\dot{\mathbf{\Theta}}^p$ described in (3.12) is an analytic expression containing terms with the general form

$$a_k \sin(\omega k) + b_k \cos(\omega k)). \tag{3.24}$$

Seeing as the frequency ω is constant we can similar to [12] formulate the integral of (3.24) at time instance k as

$$a_k \frac{-1}{\omega} \cos(\omega k) + b_k \frac{1}{\omega} \sin(\omega k)). \tag{3.25}$$

By applying the general relation of (3.24) and (3.25) to all the terms in the periodic component's angular rate $\dot{\mathbf{\Theta}}^p_k$ we can express the periodic orientation component as

$$\hat{\mathbf{\Theta}}^p_k = \begin{bmatrix} \sum_{i=1}^{\varsigma} a^{\theta}_{ik} \frac{-1}{\omega^{\theta}_i} \cos(\omega^{\theta}_i k) + b^{\theta}_{ik} \frac{1}{\omega^{\theta}_i} \sin(\omega^{\theta}_i k) \\ \sum_{i=1}^{\tau} a^{\varphi}_{ik} \frac{-1}{\omega^{\varphi}_i} \cos(\omega^{\varphi}_i k) + b^{\varphi}_{ik} \frac{1}{\omega^{\varphi}_i} \sin(\omega^{\varphi}_i k) \\ \sum_{i=1}^{\upsilon} a^{\psi}_{ik} \frac{-1}{\omega^{\psi}_i} \cos(\omega^{\psi}_i k) + b^{\psi}_{ik} \frac{1}{\omega^{\psi}_i} \sin(\omega^{\psi}_i k) \end{bmatrix}. \tag{3.26}$$

The equivalent *linear* state space observation model for the estimated periodic orientation component $\hat{\mathbf{\Theta}}^p$ becomes

$$\hat{\mathbf{\Theta}}^p_k = O^p_k \hat{\mathbf{x}}^p_k \tag{3.27}$$

where O^p_k is the estimate observation matrix at time k defined as

$$O^p_k = \begin{bmatrix} \mathbf{o}^{\theta}_k & \mathbf{0} & \mathbf{0} & 0 & 0 & 0 \\ \mathbf{0} & \mathbf{o}^{\varphi}_k & \mathbf{0} & 0 & 0 & 0 \\ \mathbf{0} & \mathbf{0} & \mathbf{o}^{\psi}_k & 0 & 0 & 0 \end{bmatrix} \tag{3.28}$$

in which

$$\mathbf{o}^{\theta}_k = \begin{bmatrix} \frac{-1}{\omega^{\theta}_1} \cos(\omega^{\theta}_1 k) & \cdots & \frac{-1}{\omega^{\theta}_{\varsigma}} \cos(\omega^{\theta}_{\varsigma} k) & \frac{1}{\omega^{\theta}_1} \sin(\omega^{\theta}_1 k) & \cdots & \frac{1}{\omega^{\theta}_{\varsigma}} \sin(\omega^{\theta}_{\varsigma} k) \end{bmatrix} \tag{3.29}$$

$$\mathbf{o}^{\varphi}_k = \begin{bmatrix} \frac{-1}{\omega^{\varphi}_1} \cos(\omega^{\varphi}_1 k) & \cdots & \frac{-1}{\omega^{\varphi}_{\tau}} \cos(\omega^{\varphi}_{\tau} k) & \frac{1}{\omega^{\varphi}_1} \sin(\omega^{\varphi}_1 k) & \cdots & \frac{1}{\omega^{\varphi}_{\tau}} \sin(\omega^{\varphi}_{\tau} k) \end{bmatrix} \tag{3.30}$$

$$\mathbf{o}^{\psi}_k = \begin{bmatrix} \frac{-1}{\omega^{\psi}_1} \cos(\omega^{\psi}_1 k) & \cdots & \frac{-1}{\omega^{\psi}_{\nu}} \cos(\omega^{\psi}_{\nu} k) & \frac{1}{\omega^{\psi}_1} \sin(\omega^{\psi}_1 k) & \cdots & \frac{1}{\omega^{\psi}_{\nu}} \sin(\omega^{\psi}_{\nu} k) \end{bmatrix} \tag{3.31}$$

As a result of (3.14) and (3.27) both being linear state space models this means that the estimated state vector $\hat{\mathbf{x}}_k^p$ indirectly represent both the angular rate and the angle of the estimated periodic orientation component $\hat{\mathbf{\Theta}}_k^p$. The only difference between the two domains is simply which observation matrix is used.

It is also because of this that the analytic integration can be performed by nothing else than a matrix-vector gain operation[12] as opposed to the numerical method which usually involves a summation over time. This particular method for performing analytic integration also has an advantage over the numerical method since error in the analytical integration only depend on the error at time k and not any previous time instances.

3.2.2 Stationary orientation component estimation

Since the accelerometer measurements contain the direction of the earth's gravitational force it also implies the orientation of the sensor with respect to the NED frame. Because the input to the stationary orientation component filter, the accelerometer measurements, has a direct relation to the stationary orientation component $\mathbf{\Theta}^p$ a suitable state vector is the component which is to be estimated. The state vector for the stationary orientation component is therefore defined as

$$\mathbf{x}^s = \begin{bmatrix} \theta & \varphi & \psi \end{bmatrix}^T. \tag{3.32}$$

State motion model and filter prediction

Based on the observation that the stationary orientation component $\mathbf{\Theta}^s$ varies in a relatively slow and unpredictable manner we have decided to model its movement by a random walk model stated as

$$\mathbf{x}_{k+1}^s = F^s \mathbf{x}_k^s + \boldsymbol{\delta}_k^s \tag{3.33}$$

$$\boldsymbol{\delta}_k^s \sim \mathcal{N}(\mathbf{0}, D_k^s), \tag{3.34}$$

where F^s is the state transition matrix defined by an identity matrix according to

$$F^s = \begin{bmatrix} 1 & 0 & 0 \\ 0 & 1 & 0 \\ 0 & 0 & 1 \end{bmatrix}. \tag{3.35}$$

By again using the modified Euler method as previously done in (3.9) the process noise covariance matrix D_k^s can be selected as

$$D_k^s = T_s \tilde{D}^s \tag{3.36}$$

where T_s is the sampling time.

With the described process model the EKF filter prediction step at time k can be described by the algorithm

$$\hat{\mathbf{x}}_{k|k-1}^s = F^s \hat{\mathbf{x}}_{k-1|k-1}^s \tag{3.37}$$

$$P^s_{k|k-1} = F^s P^s_{k-1|k-1}(F^s)^T + D^s_k. \tag{3.38}$$

It can be noted that the result of the algorithm only is that the previous state covariance $P^s_{k-1|k-1}$ is increased by the process noise covariance D^s_k to form the predicted state covariance $P^s_{k|k-1}$. To give a more intuitive interpretation of this we can describe this as the certainty of knowing the value of the state being decreased. That is also what can be expected since the random walk model does not give any clear indication of what value the state should assume next other than that it should be in the vicinity of the previous state value. The most motivated prediction for the state is therefore the same as previous value but with a lower degree of certainty.

State measurement model and filter update

Each measurement from the accelerometer includes both the gravity acceleration $\mathbf{g}^0$ as well as any other forces caused by translational acceleration $\mathbf{f}^t$. In the present context the gravity acceleration $\mathbf{g}^0$ can be considered as constant and known in the NED frame, but the accelerometer observes it in its own orientation frame which means that the force of gravity $\mathbf{g}^0$ has to be rotated from the NED frame to the observed one. This rotation is dependent on the stationary orientation Θ^s that is to be estimated and can be performed using a DCM rotation matrix as described in Chapter 2. Knowing this allows the measured acceleration to be modelled using the relation

$$\mathbf{y}^{acc}_k = (R(\mathbf{x}^s))^T(\mathbf{g}^0 + \mathbf{f}^t) + \boldsymbol{\varepsilon}^{acc}_k \tag{3.39}$$

$$\boldsymbol{\varepsilon}^{acc}_k \sim \mathcal{N}(\mathbf{0}, E^{acc}_k). \tag{3.40}$$

The use of this model does however pose a challenge since the accelerometer can not distinguish between the two measured forces, but information regarding the stationary orientation Θ^s is given by the gravitational force and not the translational. This means that the translational force $\mathbf{f}^t$ should be removed in the ideal scenario and a solution to this would therefore be to estimate the translational force $\mathbf{f}^t$ in order to remove it. That would on the other hand increase the complexity of the filter so another solution is to assume that the translational force is of negligible size and can be ignored. Even if this argument might be somewhat faulty it can still be useful seeing the radar system is stationary meaning that any other acceleration apart from that caused by gravity should have a mean value of zero over time. This fact can be utilized when tuning the filter by reducing the process noise covariance matrix D^s_k since any translational force will cause the estimate to move around the stationary orientation with what can be compared to as increased noise. By neglecting the translational force $\mathbf{f}^t$ in (3.39) the final mathematical model describing the accelerometer measurement can be reduced to

$$\mathbf{y}^{acc}_k = (R(\mathbf{x}^s))^T\mathbf{g}^0 + \boldsymbol{\varepsilon}^{acc}_k \tag{3.41}$$

(3.41) can be translated into the nonlinear state space measurement model

$$\mathbf{y}^{acc}_k = H^s_k(\mathbf{x}^s) + \boldsymbol{\varepsilon}^{acc}_k \tag{3.42}$$

where $H_k^s(\mathbf{x}^s)$ is the nonlinear measurement matrix defined as

$$H_k^s(\mathbf{x}^s) = (R(\mathbf{x}^s))^T \mathbf{g}^0. \tag{3.43}$$

Seeing as the measurement matrix $H_k^s(\mathbf{x}^s)$ is *non-linear* it therefore needs to be linearized in the operation point, the state $\mathbf{x}_k^p$, which is defined as the 3x3 Jacobian matrix of H_k^s described by

$$H_k'^s(\mathbf{x}^s) = \left[\left(\frac{\partial R(\mathbf{x}^s)}{\partial \theta}\right)^T \mathbf{g}^0 \qquad \left(\frac{\partial R(\mathbf{x}^s)}{\partial \varphi}\right)^T \mathbf{g}^0 \qquad \left(\frac{\partial R(\mathbf{x}^s)}{\partial \psi}\right)^T \mathbf{g}^0 \right] \tag{3.44}$$

The Kalman gain K_k^s can now be calculated using

$$\mathbf{v}_k^s = \mathbf{y}_k^{acc} - H_k^s(\hat{\mathbf{x}}_{k|k-1}^s) \tag{3.45}$$

$$S_k^s = H_k'^s(\hat{\mathbf{x}}_{k|k-1}^s) P_{k|k-1}^s (H_k'^s(\hat{\mathbf{x}}_{k|k-1}^s))^T + E_k^s \tag{3.46}$$

$$K_k^s = P_{k|k-1}^s (H_k'^s(\hat{\mathbf{x}}_{k|k-1}^s))^T (S_k^s)^{-1} \tag{3.47}$$

and the measurement update at time k is then described by

$$\hat{\mathbf{x}}_{k|k}^s = \hat{\mathbf{x}}_{k|k-1}^s - K_k^s \mathbf{v}_k^s \tag{3.48}$$

$$P_{k|k}^s = P_{k|k-1}^s - K_k^s S_k^s (K_k^s)^T. \tag{3.49}$$

The estimated stationary estimates are then added to the periodic to give an estimate of the absolute angle.

4

RESULTS

The results are divided into attitude (roll, pitch) and heading estimation. Data collected from the available radar platform with sensor installed is used for evaluation. The sensor estimates are compared to the reference as an evaluation of the SBG sensor. A designed periodic filter estimating the orientation is tuned and compared to a general solution based on quaternions but also the reference system and the SBG filter.

4.1 Scenario specifications

To motivate the results from the filter evaluation it is important to consider how the testing is performed. The evaluation of long term performance is set by what duration of time where longer obviously is preferred, but a suitable upper time limit has to be set which was determined to be 15 min (900 seconds). This section describes the method of collecting data that the filters can be applied to. It also describes how the synchronization is performed and how the filter tuning is decided as well as how this affects the results.

4.1.1 Data collection

Data is collected from the reference system and the sensor simultaneous. The output rate of the reference is 10 Hz while the sensor output is collected at a rate of 100 Hz. The duration of the collected logs are each approximately 15 minutes. This corresponds to a normal timespan when the radar is used and it is enough time to see long term trends in the filter outputs. Both systems have access to GPS which means that for time synchronization GPS time can be used. GPS can provide the time with great accuracy and the systems can produce data with GPS timestamps, which leads to well synchronized measurement points.

4.1.2 Misalignment correction

To be able to use the reference system the evaluated sensor and filter needs to be defined in a coordinate system as close as possible to the one of the reference. This means that before logging any data the misalignment between the sensor and the reference needs to be compensated for. The misalignment angle α can be seen as a very important tuning parameter since if the two systems are measuring roll, pitch and heading in two different coordinate systems it is meaningless to compare them. In the test situation for the radar platform described earlier the coordinate system for the sensor is located as in Figure 1.5. The misalignment angle α is unknown but can be obtained by taking observing angular measurements when the whole system is still. The reference system is not completely perpendicular relative the ground which means that there is an initial pitch angle β_{ref} as shown in the leftmost illustration in Figure 4.1. Since positive direction of pitch angle is defined in different directions between the two systems, the SBG sensor will measure an angle β_{sbg}. The two measurement angles are added to remove the angle relative to ground as

$$\beta'_{sbg} = \beta_{ref} + \beta_{sbg} \tag{4.1}$$

where β'_{sbg} is the relative difference between the two coordinate systems. This gives the situation in the middle illustration in Figure 4.1. Then the misalignment angle α easily can be calculated as

$$\alpha = 90^\circ - \beta'_{sbg}. \tag{4.2}$$

The last step is then to define the axes in the same orientation as the reference system as

$$x'_{sbg} = -z_{sbg}, \quad y'_{sbg} = -y_{sbg}, \quad z'_{sbg} = -x_{sbg}. \tag{4.3}$$

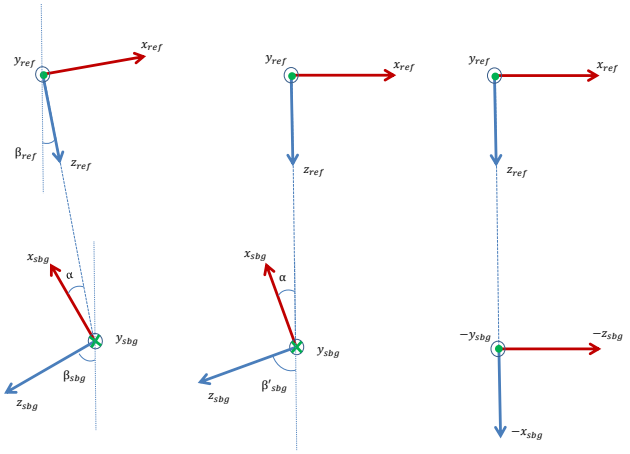

Figure 4.1: Illustration of misalignment between two coordinate systems.

In Figure 4.2a a measurement sequence of roll and pitch angle before calculation of α is shown. The pitch outputs here corresponds to β_{ref} and β_{sbg}. The mean values of this data are used in (4.1)-(4.3) to calculate the misalignment and rotate the axis into the correct position. After the compensation with α the measurements look like those in Figure 4.2b. Now the angle outputs are more consistent between the systems.

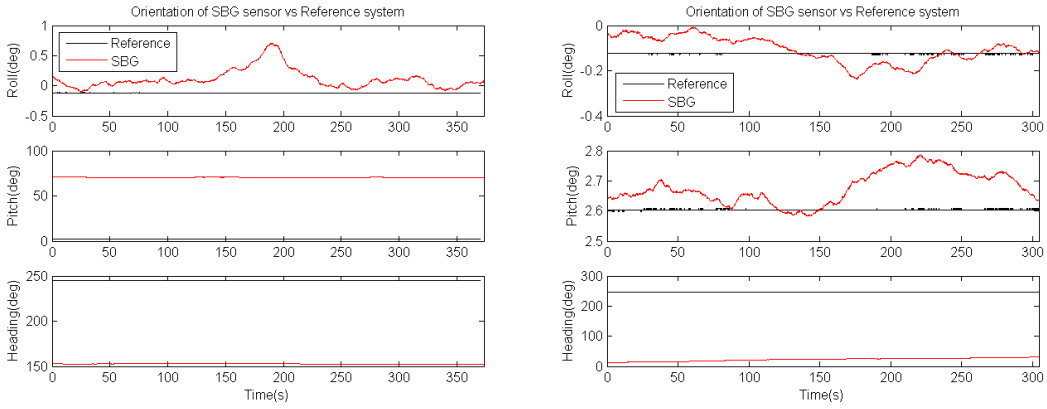

(a) Before correction for misalignment. **(b)** After correction for misalignment with α.

Figure 4.2: The coarse misalignment correction.

However when measuring the filter output from the SBG sensor compared to the

reference it can be seen in Figure 4.3a that there still is a small offset due to misalignment. This fine misalignment is solved by observing pitch values from the SBG and the reference, the mean difference is here measured to be 0.092°. By using this angle and forming a rotation matrix as introduced in Chapter 2, a matrix describing a rotation of 0.092° in pitch is obtained. The raw sensor data is then transformed to a more correct coordinate system. For the gyroscope the transformed data can be expressed as

$$\mathbf{y}^{gyr} = R(0,0.092,0)\mathbf{y}^{gyr'} \tag{4.4}$$

where $\mathbf{y}^{gyr\prime}$ is the measured data that needs to be rotated. The accelerometer data is rotated with the same rotation matrix as

$$\mathbf{y}^{acc} = R(0,0.092,0)\mathbf{y}^{acc'} \tag{4.5}$$

For a fair comparison of any filter using raw sensor data and the already implemented SBG filter, the SBG filter output needs to be transformed to the correct system as well. This is not trivial but can be done by expressing the orientation in terms of a DCM matrix as

$$\Theta^{DCM'} = R(\theta,\varphi,\psi) \tag{4.6}$$

then instead of rotating a vector, the DCM matrix are rotated with the same rotation matrix as in REF. This corresponds to instead of rotating a vector in the sensor frame, the actual sensor frame is rotated to the reference frame as

$$\Theta^{DCM} = R(0,0.092,0)\Theta^{DCM'} \tag{4.7}$$

The rotation of a DCM matrix yields another DCM matrix that needs to be expressed as Euler angles. This is easily done as described in [6]

$$\theta = \arctan(\frac{\Theta_{32}^{DCM}}{\Theta_{33}^{DCM}}) \tag{4.8}$$

$$\varphi = \sin^{-1}(\Theta_{31}^{DCM}) \tag{4.9}$$

$$\psi = \arctan(\frac{\Theta_{21}^{DCM}}{\Theta_{11}^{DCM}}) \tag{4.10}$$

that gives the roll, pitch and heading Euler angles but now in the reference coordinate system. The results from the fine misalignment of 0.092° is shown in Figure 4.3b, now the measurements are centred around the reference axis instead of offsetted. By rotating the measurements small static errors can be compensated for but there is no way of measuring the exact misalignment angle there will always be some small error due to misalignment. Since the measured angles are extremely small a small misalignment is more dominant than if the measured angles were larger. This is of course a problem when validating results from filtering but it is known that the small remaining misalignment error is static which means that at least the dynamic error is easy to observe.

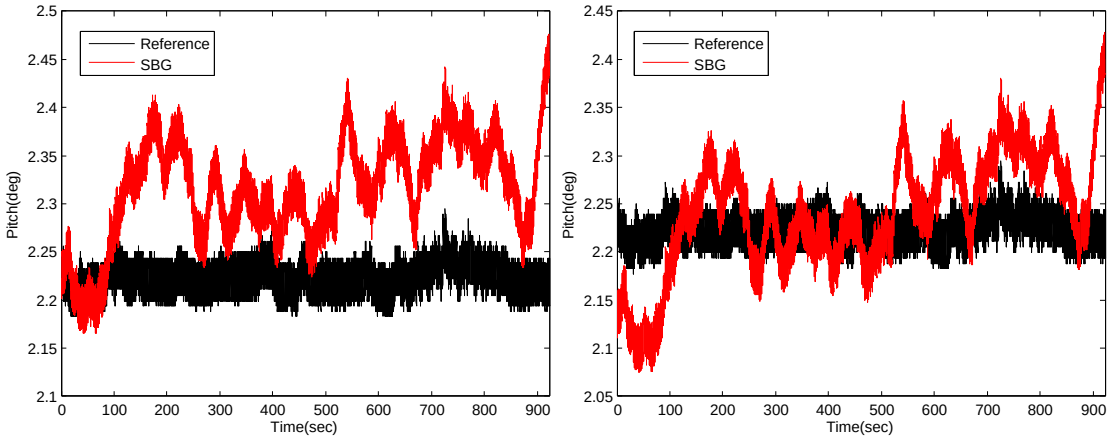

(a) Before fine misalignment. **(b)** After fine misalignment.

Figure 4.3: Results from the correction for fine misalignment. The measurements are now centred around the reference axis.

4.1.3 Parameter choices/Tuning

For the Kalman filter to work the noise parameters are assumed to be normally distributed with some mean and variance. The measurement noise E is easily classified by letting the system stand still (no antenna rotation) and observing the raw sensor data from both the gyroscopes and the accelerometers. In Figure 4.4 the distributions of the gyroscope measurements with the sensor still. The histograms show typical normal distributions which means that the Kalman filter introduced in Chapter 2 can be used. As expected the histograms shows that the gyroscopes contains biases, but this is not a problem since the implemented filter uses a bias estimator.

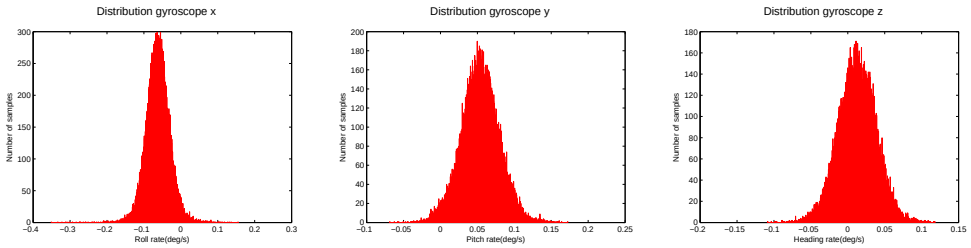

(a) Histogram gyroscope x. **(b)** Histogram gyroscope y. **(c)** Histogram gyroscope z.

Figure 4.4: Distributions for gyroscopes.

From the distributions in Figure 4.4 the covariance matrix describing the gyroscope

measurement noise is calculated to

$$E^{gyr} = \begin{bmatrix} 3.0355 \cdot 10^{-7} & 1.3016 \cdot 10^{-8} & 5.2566 \cdot 10^{-9} \\ 1.3016 \cdot 10^{-8} & 1.9341 \cdot 10^{-7} & -1.0519 \cdot 10^{-8} \\ 5.2566 \cdot 10^{-9} & -1.0519 \cdot 10^{-8} & 1.9226 \cdot 10^{-7} \end{bmatrix} \tag{4.11}$$

In the same way as the gyroscope measurements the accelerometer measurements from the same measuring sequence can be illustrated with histograms as in Figure 4.5.

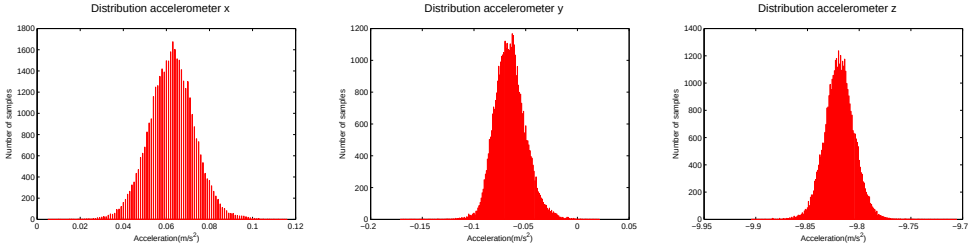

(a) Histogram x. **(b)** Histogram y. **(c)** Histogram z.

Figure 4.5: Distributions for accelerometers.

Also here the noise seems normal distributed and the covariance matrix for the accelerometer noise is calculated as

$$E^{acc} = \begin{bmatrix} 1.1630 \cdot 10^{-4} & 2.5361 \cdot 10^{-5} & 2.0552 \cdot 10^{-6} \\ 2.5361 \cdot 10^{-5} & 2.3213 \cdot 10^{-4} & -8.8820 \cdot 10^{-6} \\ 2.0552 \cdot 10^{-6} & -8.8820 \cdot 10^{-6} & 2.1310 \cdot 10^{-4} \end{bmatrix} \tag{4.12}$$

To be able to measure orientation relative ground the accelerometers are used to find the nominal gravity vector and estimating how they are tilted. For this to work, the nominal gravity vector must be defined as a tuning parameter. This is done by collecting data from the accelerometers when the sensor is installed and radar platform is still. For each instance of time the magnitude of the acceleration vector is determined and in the end the mean values of the magnitudes are calculated. This value is in this case -9.8297 m/s^2. If the sensor was perfectly placed relative ground there would only be acceleration in z and the corresponding gravity vector is chosen as

$$\mathbf{g}^0 = \begin{bmatrix} 0 \\ 0 \\ -9.8297 \end{bmatrix} \tag{4.13}$$

Until now more general tuning parameters are described but to achieve the best performance of the filter derived in Chapter 3 some other parameters needs to be tuned. The main tuning parameter of the periodic filter is which frequencies the BMFLC algorithm

can use to build the estimated signal. These frequencies are determined by investigating the raw data from the SBG sensor installed in the radar platform. By performing fast Fourier transform (FFT) on this signal any dominating frequency is found. Figure 4.6a shows the full frequency spectrum of 50 Hz for the three angular velocities. In these figures the DC component is removed. The magnitude of the frequency content is here normalized to 1 and it is clear that in roll and pitch there is one distinct frequency dominating the spectrum. This frequency is approximately 1 Hz and comes from the fact that the radar antenna is rotating with 1 Hz causing the platform to sway. Five frequencies in each axis are selected for the periodic filter. Apart from the dominating frequency two additional frequencies in each direction is used to allow some deviations from the main frequency. The selected frequencies are illustrated as stems in Figure 4.6b. In heading there seems to be no single dominating frequency but several dominating frequencies. This means that for tuning the BMFLC filter the five largest frequency components are chosen for the frequency tuning.

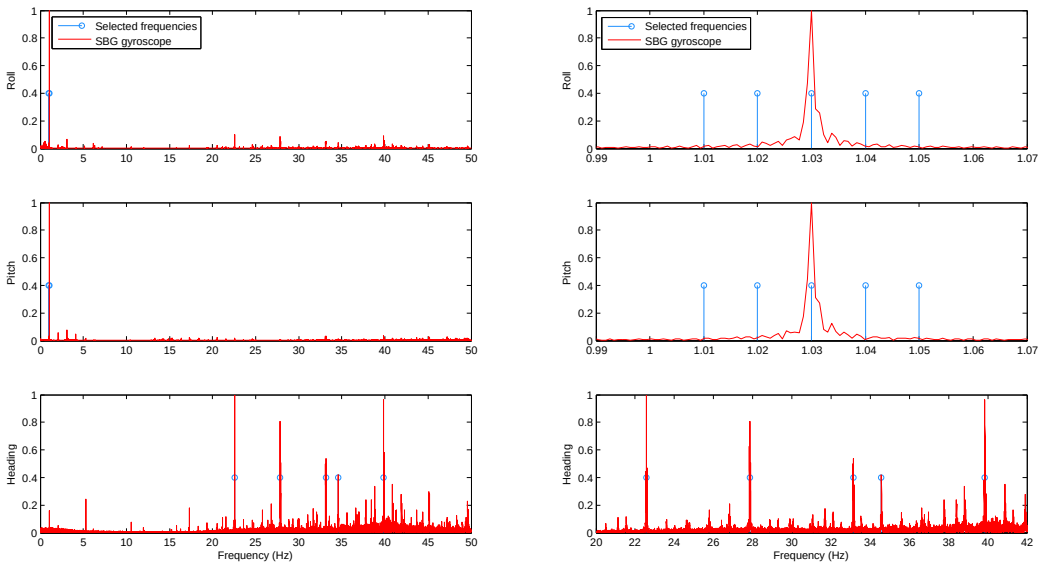

(a) Full spectrum. **(b)** Selected frequencies.

Figure 4.6: Frequency content of measured rotation rate.

The last tuning parameter to complete the filter is the process noise for the states. The states are divided into three parts: the amplitudes, the biases and the stationary angles. The amplitudes are assumed to be more or less constant but if the amplitude changes, the filter will need to be able to estimate this change. The estimated bias is assumed to be even slower due to high bias stability. The process noise for the states describing amplitude weights and bias is selected as

$$D_k^p = T_s \tilde{D}^p = 0.01 \begin{bmatrix} I_{2(\zeta+\tau+\nu)} \cdot 10^{-2} & \mathbf{0} \\ \mathbf{0} & I_3 \cdot 10^{-7} \end{bmatrix} \tag{4.14}$$

The stationary angle describes in some sense the base orientation that the radar platform moves around. This orientation is in the ideal case not changing but reference data shows that this is not the case. However this movement is very slow and the process noise is assumed to be as low as

$$D_k^s = T_s \tilde{D}^s = 0.01 I_3 \cdot 10^{-5} \tag{4.15}$$

4.2 Filter evaluation

This thesis is mainly focused on two things: evaluate the sensor directly and present some solution to take advantage of the situation that the sensor is placed in to improve estimates in orientation. The results will here be presented first in attitude (roll, pitch) and then in heading, this since the methods differ for these two cases. The results from the periodic filter will be compared to the reference and the QEKF will be used as a baseline for comparing the periodic filter with.

4.2.1 Attitude estimation

In the sensor there is an already implemented extended Kalman filter (EKF). This filter is developed by SBG and the specifications for orientation presented in Chapter 1 is based on this. How this filter works in detail is unknown but for evaluation purposes it is interesting to examine the filter output compared to the reference. The sensor has the capability to output angular measurements directly and it is therefore interesting to investigate the gain of implementing a more complex filter using raw sensor data. In Figure 4.7 the filter output in attitude(roll, pitch) from the SBG sensor are compared to the output from the reference system. As can be seen, the roll angle from the sensor follows the reference's dynamic but the absolute angle seems to be less accurate. In Figure 4.7d the error between the SBG filter and the reference is shown. It can be seen that the error from SBG is less than $\pm 0.2^\circ$ which also corresponds to the specified error of the sensor.

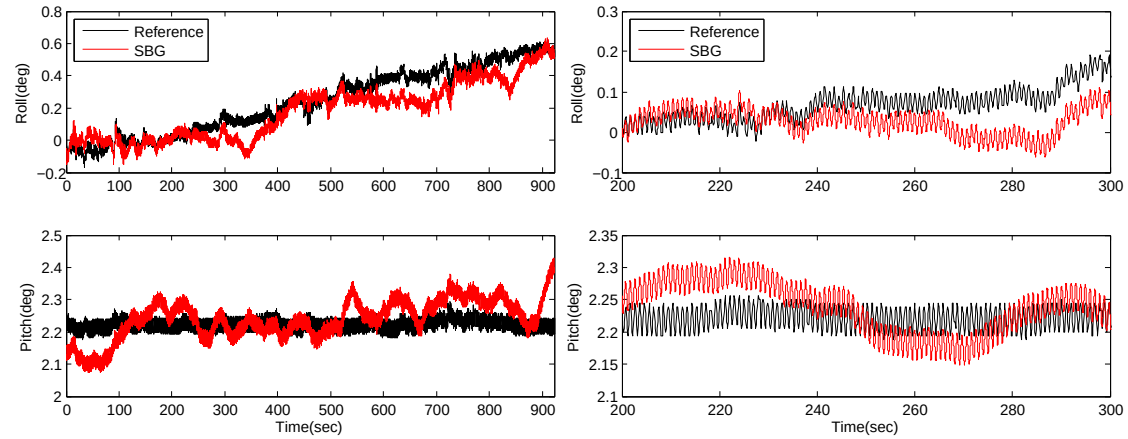

(a) Complete log of 900 s window.

(b) Zoomed in to 100 s window.

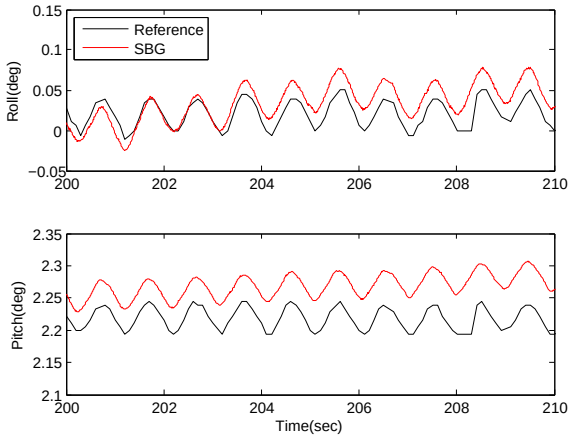

(c) Zoomed in to 10 s window.

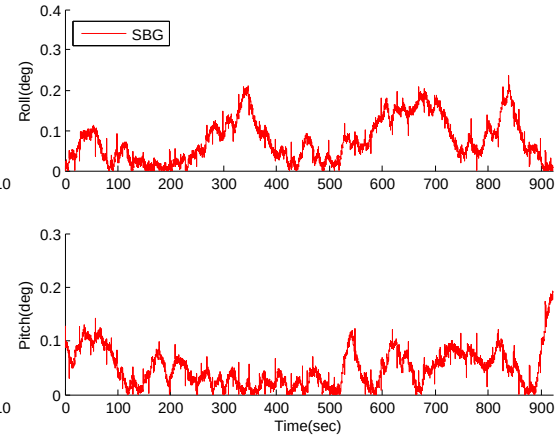

(d) SBG absolute error from reference.

Figure 4.7: SBG filter vs Reference system output.

There is a drifting behaviour in the estimated angles, but the dynamic behaviour of does however follow the reference's dynamic behaviour. This can be seen more clearly in the 10 second window in Figure 4.7c. If the drift behaviour was then removed it is reasonable to believe that the EKF is a good solution when it comes to estimating the attitude.

The periodic filter described in Chapter 3 estimates the dynamic angle, the stationary angle and the biases of the gyroscopes. This should provide a filter solution that if a periodic motion is observed give good estimates on the absolute angle. That is both the stationary and periodic angle should correspond to the motion of the platform measured by the reference system.

The amplitudes of the estimated angular velocity signal can be visualized using the amplitude states as described in (2.59). In Figure 4.8a periodic angular rate measurements from the gyroscope together with the estimated angular velocity is shown. The estimated amplitudes for each of the five selected frequencies are depicted in Figure 4.8b and as expected there is one amplitude in roll/pitch that is more dominant than the others. This amplitude are the one corresponding to the dominant frequency in the FFT plot in Figure 4.6. Since the additional four frequencies surrounding each of the dominant ones in roll and pitch have a very low amplitude their usefulness can be questioned as they do not seem to add any robustness.

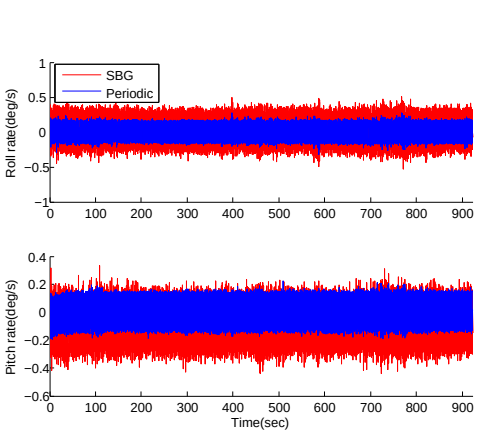

(a) Gyroscope signal(red) and estimate.

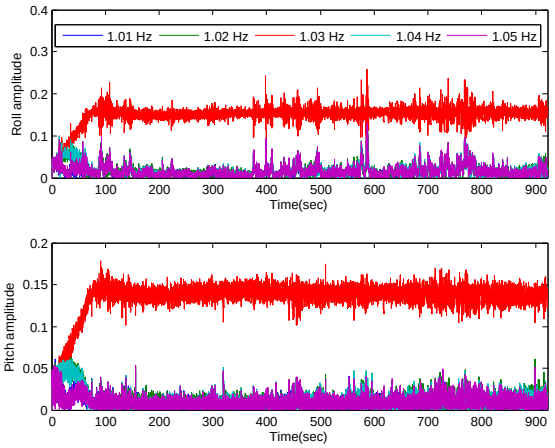

(b) Amplitude estimates of the frequencies in roll and pitch.

Figure 4.8: Estimates illustrated as angular velocity and amplitudes.

As seen from the distributions of gyroscope measurements in Figure 4.4 there is some bias of the sensors that needs to be removed for best estimation. In Chapter 3 the bias estimator is explained that finds the biases and then subtracts them to form the best possible estimation of the angular rate. The mean angular rotation of the platform should be zero since it is not moving from its starting point. In Figure 4.9 the measurements of angular rotation and the estimated biases are shown.

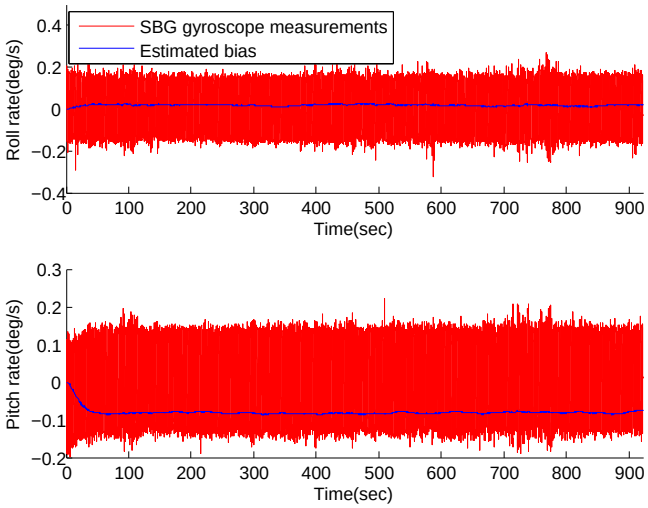

Figure 4.9: Raw gyroscope data and estimated bias.

With the bias and the amplitudes estimated the angular velocity estimate can be formed. Figure 4.10 shows the estimates from Figure 4.8a zoomed in to a window of 10 seconds. Here the power of the periodic filter is shown. All frequencies except the one defined in the FFT is neglected and what is left is a smooth signal representing the angular velocity. The estimated velocity is centred around 0 $^\circ/s$ which is an additional indication that the bias estimation works.

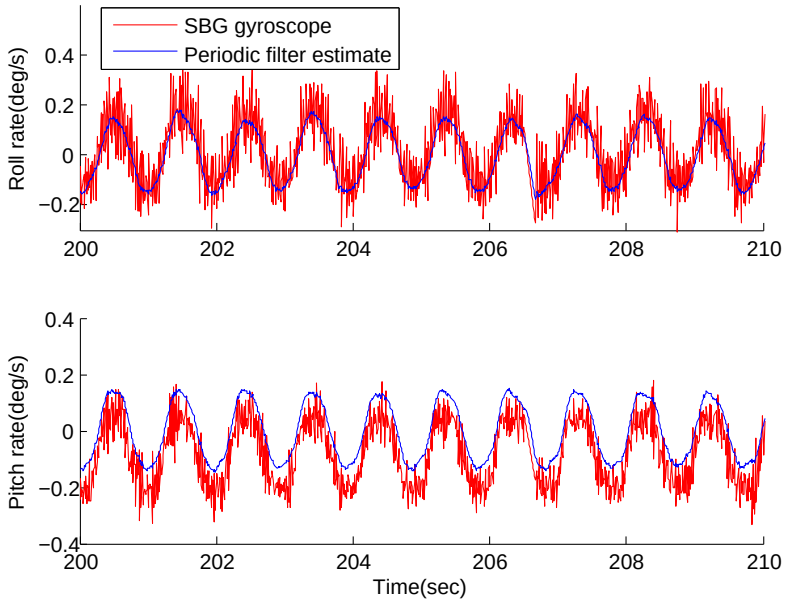

Figure 4.10: Raw gyroscope data and estimated angular velocity.

When assuming the periodic motion it is assumed that the drift observed in the SBG estimates is not an actual motion and the platform is moving around a stationary base angle. This base angle however are not assumed to be fixed but is determined in the filter estimating this stationary angle Θ^s. This assumption is intended to improve the orientation estimates compared to a more general method such as the QEKF derived in 2. In Figure 4.11a these two filters are compared to the reference. It is clear that the periodic filter is performing better than the QEKF, especially by inspecting Figure 4.11d where the error for the both filters are plotted. The error from the QEKF is in static error bigger than the periodic and also the dynamic error is worse for the QEKF where the error spans from 0 to 0.4 ° in roll and 0 to 0.2 ° in pitch. The error from the periodic filter is more stable from 0 to 0.1 ° in roll and 0 to 0.05 ° in pitch. The reason that the pitch error is smaller is due to the fact that the movement in pitch is about half of the movement in roll

The results show that the periodic filter is estimating the attitude better than a simple more general solution. This is an important observation since it shows that it actually can be worth developing a more complex filter that uses information of motion to improve orientation estimation atleast compared to the general solution.
The assumption of slowly changing amplitudes seems to be correct which means that the low process noise is well motivated. the static angle is also slow varying but the low noise on this tuning parameter causes the filter to have a long transient period as seen

in Figure 4.11a. This is of course a disadvantage with the implemented periodic filter but in radar applications the accuracy is way more important so the 80 seconds long transient time is worth the wait if the filter produces stable accurate results after that.

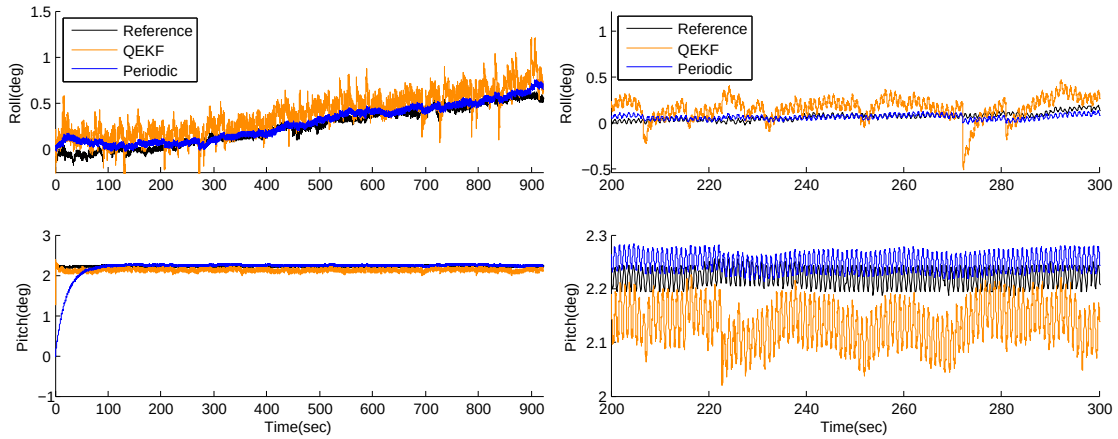

(a) Complete log of 900 s.

(b) Zoomed in to 100 s window.

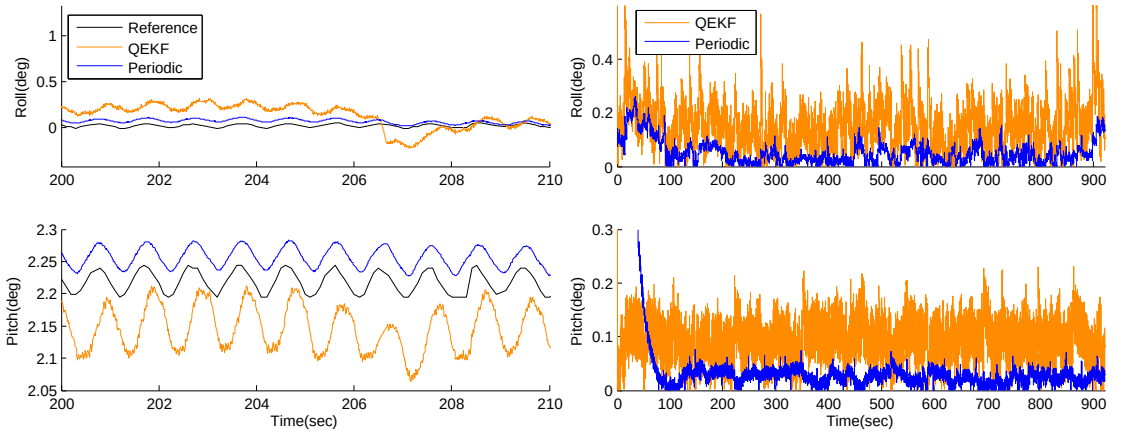

(c) zZoomed in to 10 s window.

(d) Absolute error of periodic filter and QEKF.

Figure 4.11: Periodic vs QEKF filter and Reference system.

In Figure 4.12a the periodic filter is compared to the SBG filter outputs in the sensor. It is clear that the periodic filter estimates are comparable with the SBG estimates. The periodic filter has one great advantage over the SBG filter and that is that due to the assumption of periodicity it does not drift. The drift observed in the SBG output results in an error that changes over time. The error from the periodic filter is however not drifting due to the analytical integration. The stable error from the periodic filter is

mainly due to some small remaining misalignment between the SBG sensor and the reference.

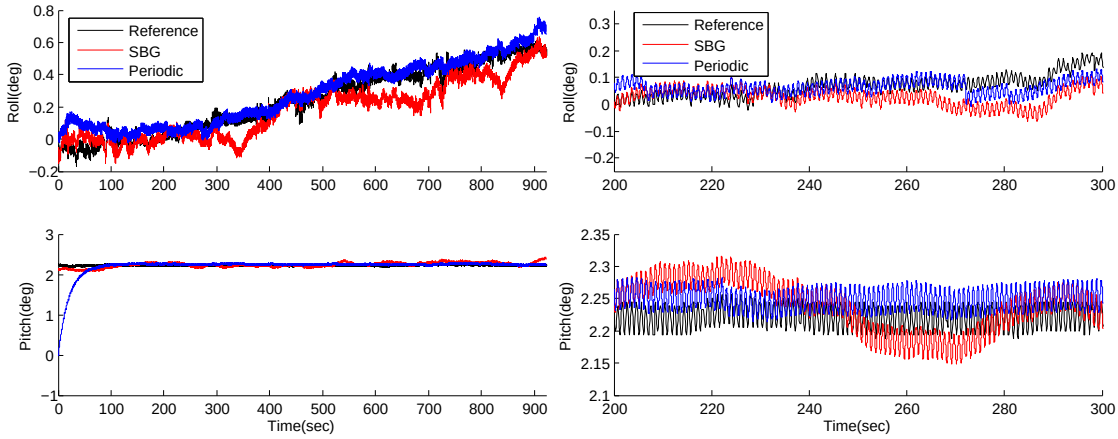

(a) Complete log of 900 s.

(b) Zoomed in to 100 s window.

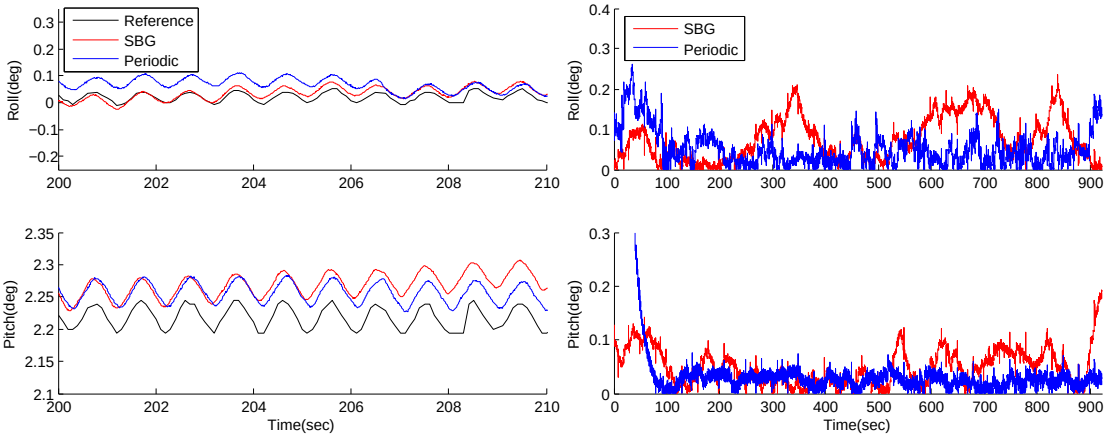

(c) Zoomed in to 10 s window.

(d) SBG and periodic filter absolute error.

Figure 4.12: Periodic vs SBG filter and Reference system.

To quantify the results from the filter comparison root mean square deviation (RMSD) [32] is used, this is a way of determining the standard deviation of the error and is calculated as

$$RMSD = \sqrt{E[\mathbf{y}^{ref} - \hat{\Theta}]^2} \tag{4.16}$$

where $E[]$ corresponds to the expected value. In Table 4.1 the RMSD values for the three filters are shown and it is seen that the periodic filter outperforms both the general QEKF and also the SBG solution.

Table 4.1: RMSD values from 800 s long data sequences where The initial transients are excluded.

RMSD	SBG	Quaternion EKF	BMFLC
Roll	0.0927	0.1757	0.0509
Pitch	0.0595	0.1888	0.0282

4.2.2 Heading estimation

The method for testing and evaluating heading angle is the same as for attitude. A pure comparison between the SBG filter and the reference is shown in Figure 4.13. As seen the reference heading is more or less constant while the SBG output is monotonically decreasing. This is a not entirely unexpected behaviour since it is known that the SBG filter uses magnetometers to estimate heading and the rotating antenna disturbs the magnetic fields. The measured magnetic field is shown in Figure 4.13b and as seen it is not constant but periodically distorted as expected which means that it cannot be compensated with calibration. To compensate for the distortions in magnetic field it is possible to use the fact that it is known to be constant and remove all periodic measurements and hence get only the constant level.

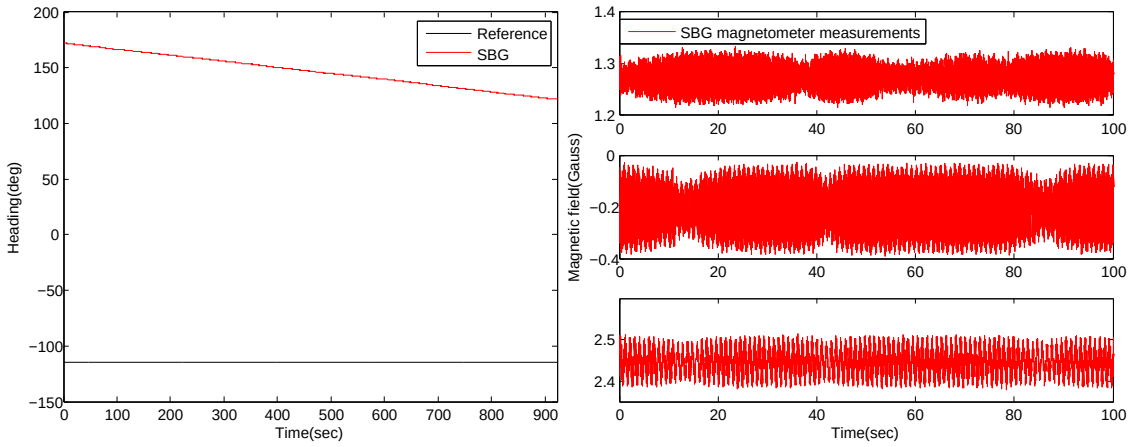

(a) Complete log of 900 s. **(b)** Magnetometer data from the first 100 s.

Figure 4.13: Comparison of heading and magnetometer data from SBG.

For the periodic filter the amplitudes in heading are harder to interpret since now there is not one dominating frequency. In Figure 4.14b the amplitudes of heading rate is illustrated in the same way as for the attitude. In this case amplitude weights for other frequencies than the strongest are influencing the estimated angular velocity. The amplitudes describe how much of each frequency component that is present in the signal

since the estimated signal is a sum of sine waves with the amplitudes in Figure 4.14b and with corresponding frequency.

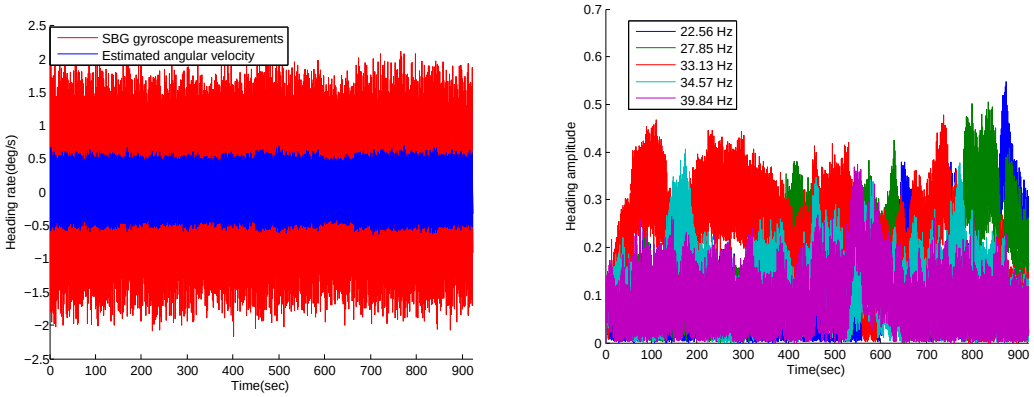

(a) Gyroscope signal(red) and estimate.

(b) Amplitude estimate for the five frequencies in heading.

Figure 4.14: Estimates illustrated as angular velocity and amplitudes.

For the bias estimation there is no difference between attitude and heading since it is only gyroscope measurements around different axis and the periodicity does not affect the bias. This is confirmed in Figure 4.15 where the bias is estimated just as good in heading as attitude.

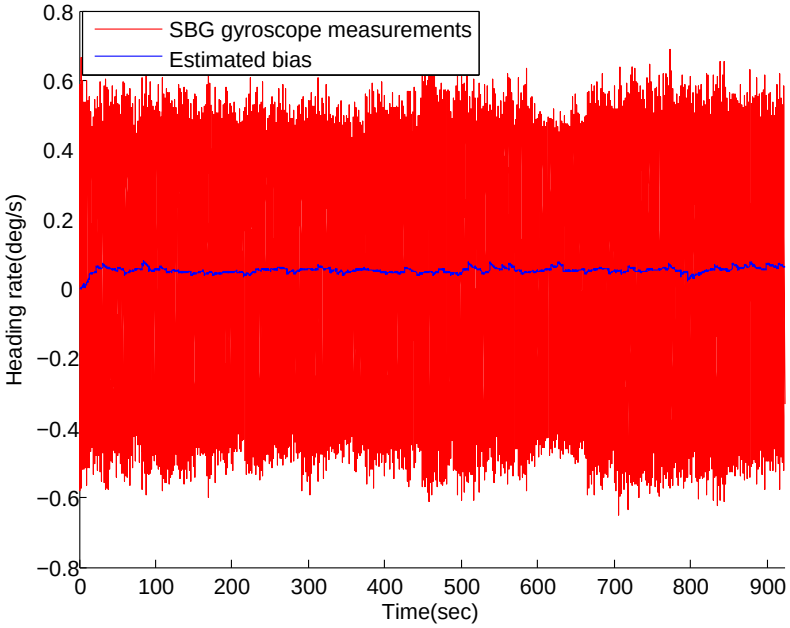

Figure 4.15: Raw gyroscope data and estimated bias of heading rate.

Figure 4.16 shows a 10 second window of the gyroscope measurements and the estimated heading rate. In this figure there is no smooth signal as in the attitude case and that is of course because the estimated angular velocity no longer consist of a signal with more or less one frequency. It is hard to see but the estimated signal is a periodic signal consisting of the frequencies chosen for tuning which means that the noise is filtered out leaving only the motion.

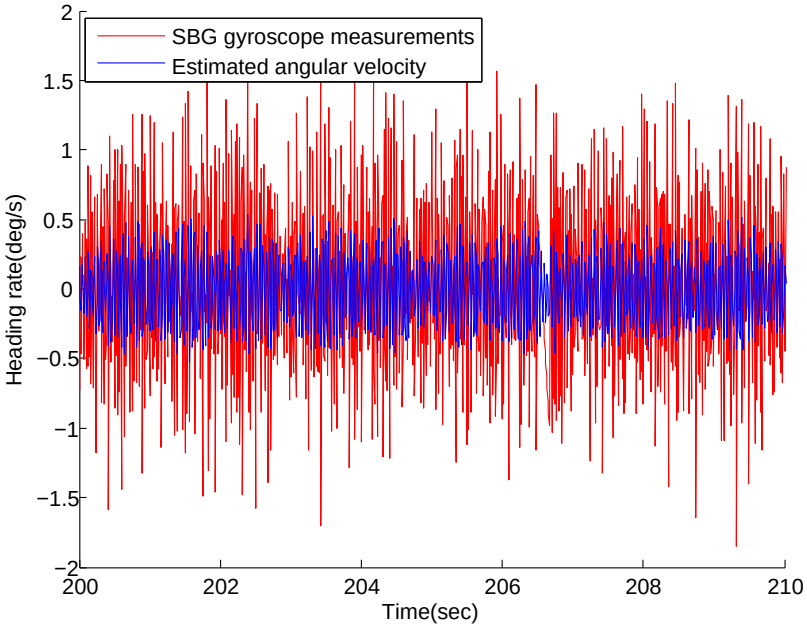

Figure 4.16: Raw gyroscope data and estimated angular velocity.

The periodic filter does not use magnetometers since this is known to cause problems. Therefore the filter is not able to resolve the absolute heading of the sensor which leads to that the estimated heading will always be centred around 0° which is verified in Figure 4.17. However if heading movement is periodic and the mean velocity is zero, the periodic filter can be used to estimate the dynamic heading. That is how much the heading moves but not around which stationary angle it moves. In Figure 4.17 the mean of the reference signal is removed for easier comparison with the dynamics in the periodic filter. The estimates from the periodic filter are not consistent with the reference and the dynamic behaviour is not the same either. The reference system has an output rate of 10 Hz meaning that frequencies higher than 5 Hz is not observable, which means that the frequencies from the SBG gyroscope data of 22.5 Hz and up to 40 Hz is not possible to see in the reference signal. It is therefore impossible to see the true motion in the reference and comparing the dynamics is useless. As it is there is no way of telling how good the estimated heading is with the available reference system.

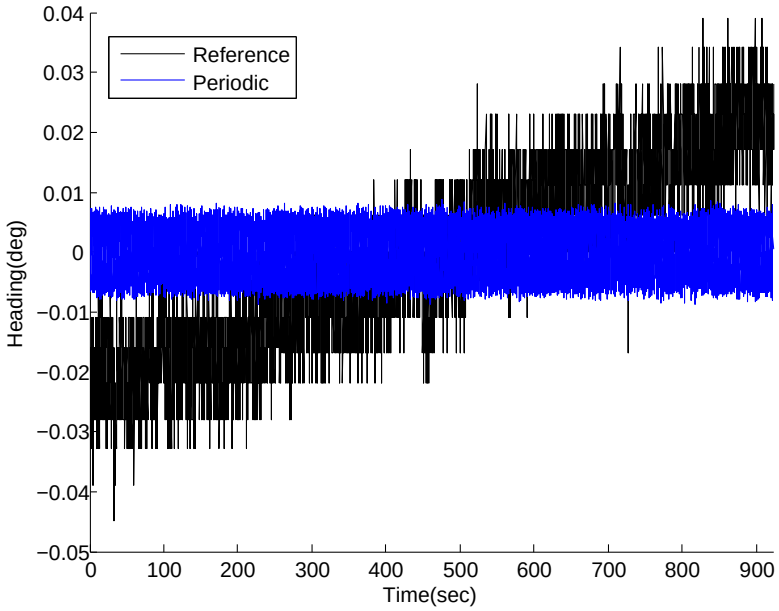

Figure 4.17: Periodic vs Reference heading with mean removed.

5

CONCLUSION

The evaluation of the SBG sensor shows that the specified accuracy in attitude is fulfilled, the angular estimates are never further from the reference system than 0.2°. There is however a drifting behaviour in the estimates most likely due to that the filter is general and not tuned for radar platforms. In heading the SBG estimates are drifting due to that the sensor is placed in an environment that distorts the magnetometers used for this estimation.

The periodic filter designed shows that it, despite simplifications regarding modelling and tuning, can be worth defining a periodic model for the type of system being evaluated. Compared to a general solution using quaternions it shows improved results. When compared to the SBG filter the periodic filter is better, especially the drift obtained in the SBG estimates is not present in the output of the periodic filter. The analytical integration of estimated velocity is a good solution when the properties of the motion are known because the numerical integration is avoided and thereby also drift.

There is a small static error remaining in the periodic filter due to problems in measuring an exact misalignment angle. In heading gyroscope data shows that there seems to be frequencies of 22.5-40 Hz in the heading motion. But since the reference only shows frequencies up to 5 Hz it is impossible to determine the performance of the periodic filter in heading to any further extent.

A major advantage of the periodic filter is in how it divides the stationary and periodic components of the estimates. This separation is currently only done to filter out the periodic part of the angular rate from the gyroscopes. A possibility is however to use the same concept of separation to eliminate any periodic component of the accelerometer measurements which currently interfere with the estimated stationary of the orientation. This issue is currently dealt with by tuning of the stationary orientations process noise that has the disadvantage of also making it slow in the initial convergence during filter initialization. Even if it has not been investigated there is also the possibility that remov-

ing the periodic component of the magnetometer could remove much of the disturbance meaning that heading may be able to be estimated.

As a final remark it can be said that the MEMS-based inertial navigation system Ellipse-N does not provide a complete solution for the orientation when used in radar applications. A partial solution such as the roll and pitch or relative movement of those can however be obtained reliably meaning that MEMS-based sensors can be used as a complementing system.

Bibliography

[1] Saab, Giraffe amb air surveillance and ground-based air defence, http://saab.com/globalassets/commercial/land/force-protection/sense-and-detect/giraffe-amb/giraffe_amb_a4.pdf, accessed: 2015-06-15.

[2] G. Wang, L. Chen, S. Jia, Optimized bias estimation model for 3-d radar considering platform attitude errors, Aerospace and Electronic Systems Magazine, IEEE 27 (1) (2012) 19–24.

[3] Y. Yang, J. Farrell, Magnetometer and differential carrier phase gps-aided ins for advanced vehicle control, Robotics and Automation, IEEE Transactions on 19 (2) (2003) 269–282.

[4] VectorNav, Inertial measurement units and inertial navigation, http://www.vectornav.com/support/library/imu-and-ins, accessed: 2015-06-15.

[5] Xsens, Inertial sensors overview, https://www.xsens.com/tags/inertial-sensors/, accessed: 2015-06-14.

[6] A. Guinamard, Ellipse AHRS & INS User Manual, SBG systems.

[7] Sagem, Navigation systems, http://www.sagem.com/aerospace/military-aircraft/navigation-systems, accessed: 2015-06-16.

[8] Sbg, Ellipse development kit, http://www.sbg-systems.com/products/ellipse-development-kit, accessed: 2015-06-16.

[9] S. O. Madgwick, An efficient orientation filter for inertial and inertial/magnetic sensor arrays, Ph.D. thesis, University of Bristol (2010).

[10] B. Zhang, et al., Beamforming for wireless communications between buoys, in: Oceans - San Diego, 2013, 2013, pp. 1–6.

[11] S. Tully, et al., Monocular feature-based periodic motion estimation for surgical guidance, in: Robotics and Automation (ICRA), 2013 IEEE International Conference on, 2013, pp. 4403–4408.

[12] K. C. Veluvolu, W. T. Ang, Estimation of Physiological Tremor from Accelerometers for Real-Time Applications, Sensors Journal (11) (2011) 3020–3036.
URL http://www.ncbi.nlm.nih.gov/pmc/articles/PMC3231635/pdf/sensors-11-03020.pdf

[13] J. Esfandari, et al., Introduction to mems gyroscopes, http://electroiq.com/blog/2010/11/introduction-to-mems-gyroscopes/, accessed: 2015-06-02.

[14] D. Titterton, J. Weston, Strapdown Inertial Navigation Technology, 2nd Edition, IET Radar, Sonar, Navigation and Avionics, The institution of electrical engineers, United Kingdom, 2004.

[15] H. Arditty, Estimation of Physiological Tremor from Accelerometers for Real-Time Applications, Optics letters 6 (8) (1981) 401–403.
URL http://www.opticsinfobase.org/ol/abstract.cfm?uri=ol-6-8-401

[16] Y. Korkishko, et al., Strapdown inertial navigation systems based on fiber-optic gyroscopes, Gyroscopy and Navigation 5 (4) (2014) 195–204.
URL http://link.springer.com/article/10.1134%2FS2075108714040154

[17] S. Chao, et al., Lock-in Growth in a Ring Laser Gyro, Physics of Optical Ring Gyros 0487 (50) (1984) 50–57.
URL http://proceedings.spiedigitallibrary.org/proceeding.aspx?articleid=1237746

[18] Mems accelerometer, http://www.instrumentationtoday.com/mems-accelerometer/2011/08/, accessed: 2015-06-02.

[19] F. Tejada, Silicon on Insulator CMOS and microelectromechanical systems: mechanical devices, sensing techniques and system electronics, Ph.D. thesis, John Hopkins University.

[20] VectorNav, Gyroscope, http://www.vectornav.com/support/library/gyroscope, accessed: 2015-06-04.

[21] W. Stockwell, Angle random walk, http://www.moog-crossbow.com/Literature/Application_Notes_Papers/Angle_Rom_Walk_Estimation_for_Rate_Gyros.pdf, accessed: 2015-05-27.

[22] W. Stockwell, Bias stability measurement: Allan variance, http://www.moog-crossbow.com/Literature/Application_Notes_Papers/Gyro_Bias_Stability_Measurement_using_Allan_Variance.pdf, accessed: 2015-06-04.

[23] CHRobotics, Understanding euler angles, http://www.chrobotics.com/library/understanding-euler-angles, accessed: 2015-06-15.

[24] D. Eberly, Rotation representations and performance issues, http://www.geometrictools.com/Documentation/RotationIssues.pdf, accessed: 2015-06-04.

[25] F. Gustafsson, Orientation Estimation using Smartphone Sensors, Automatic control, Linköping.

[26] S. Särkkä, Bayesian optimal filtering equations and kalman filter, `http://www.lce.hut.fi/~ssarkka/course_k2011/pdf/handout3.pdf`, accessed: 2015-06-15.

[27] S. Särkkä, Bayesian filtering and smoothing, no. 3, Cambridge University Press, 2013.

[28] F. Gustafsson, Statistical Sensor Fusion, GAZELLE BOOK SERVICES, 2012.
URL `https://books.google.se/books?id=JSsruwAACAAJ`

[29] G. Cazelais, Linear combination of sine and cosine, `http://pages.pacificcoast.net/~cazelais/252/lc-trig.pdf`, accessed: 2015-06-04.

[30] V. Bonnet, et al., Estimation of Physiological Tremor from Accelerometers for Real-Time Applications, Journal of NeuroEngineering and Rehabilitation 10 (29).
URL `http://www.ncbi.nlm.nih.gov/pmc/articles/PMC3620521/`

[31] L. Svensson, Selecting the discrete time motion noise covariance, `https://pingpong.chalmers.se/courseId/4231/node.do?id=1966139&ts=1410841889466&u=-963426579`, accessed: 2015-06-15.

[32] Wikipedia, Root-mean-square deviation, `http://en.wikipedia.org/wiki/Root-mean-square_deviation`, accessed: 2015-06-02.